Simulation of Liquid Entrainment in BWR Annular Flow Using an Interface Tracking Method Approach

By

Saaransh Gulati
B.Tech-M.Tech Mechanical Engineering,
IIT Kanpur (2009)

SUBMITTED TO THE DEPARTMENT OF NUCLEAR SCIENCE AND ENGINEERING IN PARTIAL FULFILLMENT OF THE REQUIREMENTS FOR THE DEGREE OF

MASTER OF SCIENCE IN NUCLEAR SCIENCE AND ENGINEERING
AT THE
MASSACHUSETTS INSTITUTE OF TECHNOLOGY
JUNE 2012

Signature of Student_____

Saaransh Gulati
Department of Nuclear Science and Engineering
05/21/2012

Approved by: _____

Prof. Jacopo Buongiorno
Associate Professor of Nuclear Science and Engineering
Thesis Supervisor

Approved by: _____

Dr. Djamel Lakehal
Research Affiliate of Nuclear Science and Engineering
Thesis Co-Supervisor

Accepted by: _____

Prof. Mujid Kazimi
TEPCO Professor of Nuclear Engineering
Chair Department Committee on Graduate Students

ACKNOWLEDGEMENTS

I would like to express my sincere gratitude to my thesis supervisor Professor Jacopo Buongiorno for his continuous support of my SM thesis and research, and for his continuous guidance and active engagement in my research work. I would also like to thank him for giving me a chance to travel to NURETH-14 conference in Canada. It was truly an amazing and very educative experience to participate and present my work in one of the best conferences in Thermal-Hydraulics.

In addition to my supervisor, I would also like to thank Dr. Djamel Lakehal for his valuable inputs and help in my learning of CFD. I really enjoyed the discussions I had with him on interface tracking and LES and they were indeed very intellectually stimulating. I would also like to thank the team at Ascomp Gmbh, Switzerland (Daniel, Chidu) for their support in customizing and adding new modules to the code to suit my research.

I would specially like to thank Dr. Despoina Chatzikyriakou (fellow research group member) for her constant support in my learning curve and suggestions in my simulations. Also, it was really nice to work with Dr. Xili Duan and Dr. Jong Won Kim on the experimental part.

A good work environment is always helpful and I would like to thank my office-mates Alex, Despoina, Dustin, Gael, Riccardo for making the office a nice and fun place to learn and work.

During the course of my stay at MIT, I have made many good friends and I would like to thank them for providing me with much needed distractions from work. I would also like to thank my parents and brother for their support and encouragement throughout my research work.

-Saaransh Gulati

TABLE OF CONTENTS

LIST OF FIGURES

LIST OF TABLES

NOMENCLATURE

LIST OF ACRONYMS

CMFD	Computational Multi-Fluid Dynamics
BWR	Boiling Water Reactors
CHF	Critical Heat Flux
NS	Navier Stokes
CFL	Courant-Friedrichs-Lewy condition
DNS	Direct Numerical Simulation
RANS	Reynolds Averaged Navier Stokes
LES	Large Eddy Simulation
LEIS	Large Eddy Interface Simulation
ITM	Interface Tracking Methods
VOF	Volume Of Fluid
LS	Level Set
WENO	Weighted Essentially Non-Oscillatory
EPRI	Electric Power Research Institute

LIST OF SYMBOLS

g	-	Acceleration due to gravity
μ	-	dynamic viscosity
μ_g	-	Vapor dynamic viscosity
μ_l	-	Liquid dynamic viscosity
ρ	-	Density
ρ_g	-	Density of saturated vapor

ρ_l	-	Density of saturated liquid
ν	-	Kinematic viscosity
ν_g	-	Vapor kinematic viscosity
ν_l	-	Liquid kinematic viscosity
$\dot{\varepsilon}$	-	Entrainment rate
$\dot{m}_l$	-	Liquid Mass Flow Rate
$\dot{m}_{lf}$	-	Liquid Film Mass Flow Rate
$\dot{m}_{ld}$	-	Droplet Mass Flow Rate
$\dot{m}_{dep}$	-	Deposition Rate
E	-	Entrainment fraction
E_m	-	Maximum Entrainment fraction
E_∞	-	Equilibrium Entrainment fraction
j_l	-	Liquid Superficial Velocity
j_g	-	Vapor Superficial Velocity
j_{gc}	-	Critical Vapor Superficial Velocity for Onset of Entrainment
k_A	-	Atomization Coefficient
k_D	-	Deposition Coefficient
C	-	Droplet Core Concentration
Re_l	-	Liquid Reynolds Number
Re_g	-	Vapor Reynolds Number
Re_τ	-	Shear Reynolds Number
We	-	Weber Number
α	-	Void Fraction
ΔP	-	Pressure Drop
a_p	-	Pressure Forcing Term
f_i	-	Interfacial friction factor
D	-	Hydraulic Diameter
t_f	-	Liquid film thickness in annular and stratified flow
S	-	Slip ratio
χ	-	Component Indicator Function
σ	-	Surface Tension
F_{ij}	-	Volume of Fluid Characteristic Fluid Function
ϕ	-	Level Set Marker Function

γ	-	Strength of capillary forces
φ	-	Capillary Stress Term
κ	-	Radius of Curvature
ζ	-	Symbol used to describe any property
$H(\phi)$	-	Heaviside Function
$\bar{H}(\phi)$	-	Modified Heaviside Function
δ	-	Grid thickness for interface relaxation
ϵ	-	Average Rate Of Dissipation Of Turbulence
η	-	Kolmogorov Length Scale
τ_η	-	Kolmogorov Time Scale
τ	-	Sub-grid Scale Stress Tensor
S_{ij}	-	Strain Rate Tensor
R	-	Sum of Convolution Induced Errors
C_s	-	Smagorinsky Model Coefficient
Δ	-	Filter Width
$G(x)$	-	Design Filter Function
f_μ^{int}	-	Turbulence Damping Function
L	-	Length of the channel
τ_w	-	Wall Shear Stress
u_τ	-	Wall Shear Velocity
y^+	-	Viscous Length Scale
y	-	Wall distance
h	-	Half Channel Width/Liquid Holdup
N_f	-	Dimensionless Property Group for Falling Liquid Films
N_λ	-	Dimensionless Wavelength for Falling Liquid Films
N_{hp}	-	Dimensionless Peak Height for Falling Liquid Films
h_o	-	Unperturbed Liquid Film Thickness for Falling Liquid Films
V	-	Velocity Scale for Falling Liquid Films
F_i	-	Interfacial Shear Force
F_{gw}	-	Vapor-Wall Shear Force
F_{lw}	-	Liquid-Wall Shear Force
τ_i	-	Interfacial Shear Stress
A_{film}	-	Interfacial Area of film

m_{core}	-	Total Mass Of Vapor Core In Stratified And Annular Flow
u_i	-	Interfacial Velocity
G	-	Mass Flux
X	-	Flow Quality
A	-	Cross Sectional Area
P_w	-	Wetted Perimeter
$\dot{q}$	-	Linear Heat Generation Rate
N_A	-	No. of Assemblies
N_P	-	No. of Pins
N_W	-	No. of Water Rods
d	-	Outer Fuel Pin Diameter
d_w	-	Outer Diameter of Water Rods
a_l	-	Assembly Inner Dimension
h_{in}	-	Inlet Specific Enthalpy
h_{out}	-	Exit Specific Enthalpy

SUBSCRIPTS

L	-	Liquid Phase
G	-	Vapor Phase

1. INTRODUCTION

1.1 Motivation:

The Boiling water reactor (BWR) system is the second most widely used nuclear reactor design used for the production of electric power. Since the BWRs essentially boil water to remove the heat produced by the nuclear fuel, a major thermal limit is dictated by the phenomenon known as critical heat flux (CHF), which in annular flow is associated with dryout of the liquid film in contact with the heated wall. This work aims at modeling the dryout conditions accurately so that the design margins could be improved thus potentially leading to an increase in power density in the BWR core.

It is noted that the flow inside a BWR core is two phase – water and steam. Since the superficial velocities of both phases are high, the flow falls in the annular regime. Dryout is defined as the condition in annular flow when there is complete removal of liquid film on the wall surface. This leads to an abrupt increase in the heat transfer coefficient and hence is not a desired condition in BWR. Dryout can only be observed in diabatic multiphase flows with high flow quality.

The liquid layer depletion leading to dryout in annular flow is due to two processes: a) Entrainment and, b) Evaporation. On the other hand, the liquid film is replenished by droplet deposition from the vapor core. Entrainment refers to the process of mechanical mass transfer from the continuous liquid field into the dispersed droplet field along an

interface. Entrainment is the dominant depletion mechanism for the liquid film under BWR operational conditions [1]. Therefore, we have chosen this phenomenon as the starting point for the development of a more general, high-fidelity modeling framework of dryout. Computational Fluid Dynamics has proved to be a very useful tool for developing high-fidelity numerical models for complex processes, making it a natural choice for modeling of entrainment phenomenon.

In addition to modeling the entrainment phenomenon, accurate modeling of different flow parameters in annular flows such as void fraction, pressure gradient, interfacial friction is also desired to achieve a complete description of the flow. Stratified flows are also very important for example in pipeline operations in upstream oil industry.

1.2 Methodology:

A number of correlations based on empirical observations for prediction of dryout conditions have been proposed in literature [2]. Most of these correlations make use of simplified assumptions, such as idealized liquid-vapor interface geometries and use of empirical coefficients to describe the interfacial exchange terms in the phase-averaged, two-fluid, six-equation model [3]. However, the interface geometry plays a major role in modeling the dryout phenomenon, and must be modeled accurately.

Interface Tracking Methods (ITM's) are a modeling technique that can be very useful for accurately capturing the sharp interfaces and interfacial features via computational means. Although this approach can be computationally expensive, in principle it eliminates the need of using empirical models for interfacial mass, momentum and scalar

exchange terms. A very limited number of studies involving multiphase flows have been carried out with the ITM approach [3]. In this work, ITMs are used for studying the entrainment phenomenon.

Level set method is one of the most commonly used ITM. The method essentially solves the Navier-Stokes equation for only one phase by assuming the density and viscosity to be discontinuous and piecewise functions of space. Since the interface topology is resolved accurately, the method is capable of predicting the formation of interfacial features very accurately.

It is also noted that flow conditions inside a BWR are highly turbulent. Under real BWR conditions the Reynolds number is relatively high ($\sim 10^5$) such that Direct Numerical Simulation (DNS) of turbulence, in which all turbulent scales are resolved, becomes computationally too expensive (as shown in appendix A). Therefore, LES Large Eddy Simulation (LES), an approach in which only the large turbulent eddies are resolved whereas the smaller eddies are modeled by means of subgrid closure relations, is a more attractive approach.

In this work, the code TransAT developed by ASCOMP Switzerland is used for carrying out the simulations. TransAT is first tested for a problem of two dimensional two phase wavy liquid films falling under gravity [4]. This exercise helps in evaluating the quality of the treatment of sharp interfaces in the code and in giving an idea of the grid sizes and solution schemes for the problem of droplet entrainment. It is noted that this problem has

some similarities with the problem of droplet entrainment. In order to test TransAT's capabilities for modeling turbulence, a benchmark case of single phase LES of simple channel flow is also carried out. The code is then used to model liquid entrainment at conditions relevant to the BWR situation using LEIS.

The first step involves accurate modeling of stratified flows. The major challenge identified in modeling such kind of flows is the use of periodic boundary conditions, which is needed to keep the grid size reasonably low. Algorithms are developed to implement proper periodic boundary conditions for treating the flow in a shorter domain without violating the underpinning physics.

After validation of stratified flow models, the modeling of annular flows is carried out. The main challenge identified here is again domain length and use of periodic boundary conditions. The simulations are first carried out for a truncated domain. Finally, a computationally expensive full domain simulation (one-full wavelength) is carried out showing that it is feasible to model entrainment using ITMs and LES. It is shown that the numerical model for a low surface tension case captures the growth of interfacial instabilities, ligament formation and detachment of liquid droplets from the liquid film.

A study comparing various macroscopic quantities such as void fraction, pressure drop, interfacial friction and entrainment fraction that can be obtained using the above simulations is also carried out and it gives reasonably good agreement with models and correlations in the literature.

1.3 Organization of Thesis:

Chapter 2 provides a review of the literature on experimental and computational work about annular flows and entrainment phenomenon. Chapter 3 and 4 provide a brief overview of the interface tracking and turbulence modeling methodologies with discussions on suitable methods required for modeling the problem of interest. Chapter 5 discusses the benchmark cases of laminar wavy falling liquid film and single phase LES of channel flow used for validating interface tracking and turbulence capabilities of TransAT. Chapter 6 describes the results obtained for stratified and annular flow simulations. Chapter 7 provides a brief summary of this work.

2. LIQUID ENTRAINMENT IN ANNULAR FLOWS

In this section, some of the characteristics of stratified and annular flows will be discussed. In addition, a discussion of liquid entrainment occurring in annular flows will also be carried out. A brief literature review focusing on different experimental and computational works that have been performed for quantifying entrainment will also be provided.

2.1 Stratified and Annular Flow:

Several different two-phase flow regimes can exist in channels and pipes depending on liquid and vapor superficial velocities. Most flow regimes are present in both vertical and horizontal channels and pipes, however, stratified flows can occur only in horizontal channels where gravity tends to separate the phases.

Figure 1 shows an illustration of stratified wavy and annular flows. In stratified flows, formation of smooth waves on the liquid-vapor interface may occur. The annular flows are characterized by formation of a liquid annular film around with a vapor core in the middle. The vapor core carries water droplets that have been torn-off (entrained) as a result of high velocity shear at the liquid film/vapor core interface.

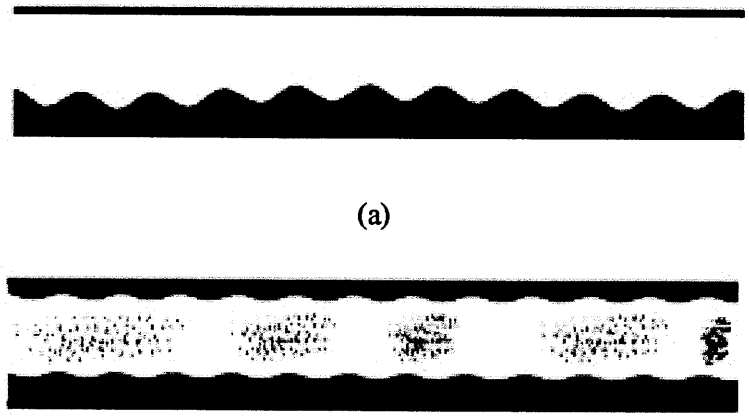

(a)

(b)

Figure 1: (a) Wavy Stratified and (b) Annular Flows

The physics behind annular flows has been of wide interest to a number of different researchers ([6], [7], [8], [9], [10]) and a number of different criteria exist for categorizing two phase flow into appropriate flow regime maps ([12], [13]). Azzopardi [14] provides a comprehensive review of different experimental techniques and influential parameters contributing to disintegration and formation of droplets occurring in two-phase flows. Azzopardi [15] gives a good overview of entrainment in churn flows. Hewitt and Hall-Taylor [16] describe experiments that the large disturbance wave is primarily responsible for droplet entrainment.

2.2 Entrainment Mechanism:

Annular flows are typically obtained for very high superficial vapor velocities and yield a very high concentration of liquid droplets in the gas core. The formation of these droplets is attributed to mass transfer between the liquid and the gaseous phase, which can occur

due to two reasons: a) evaporation (which does not lead to the formation of droplets), and b) tearing-off of the liquid film (or off) by a high velocity shear imposed by difference in velocities on either side of the interface between the gaseous and liquid phase. The process of tearing off of liquid droplets from the liquid film by the gaseous phase by the virtue of a high velocity shear constitutes the phenomenon that is known as liquid entrainment in annular flows.

From a topological viewpoint, entrainment is characterized by formation of small roll waves on top of large disturbance waves. The roll waves are the result of formation of Kelvin Helmholtz instabilities on the surface of disturbance waves due to interfacial shear. This leads to formation of liquid ligaments. The ligaments eventually disintegrate into droplets when the shear at the interface becomes very large and dominates other forces acting on the interface such as surface tension and gravity.

It is noted here that the liquid droplets entrained by the gaseous phase may re-enter the liquid core, leading to droplet deposition, which acts as a counter phenomenon to entrainment. At equilibrium (a conditions that can be achieved only in fully-developed, adiabatic annular flow), the amount of entrainment is equal to the amount of deposition.

From the above discussion, it is clear that the primary factor for initiating droplet entrainment is the interfacial shear imposed by the gas phase and the primary factor countering its effects is droplet deposition. Hence, in order to quantify entrainment, the parameters that need to be modelled are: a) conditions when entrainment starts and b)

entrainment and deposition rate. The measurement of size of entrained droplets is also important as it affects the rate of deposition.

The entrainment rate, denoted by $\dot{\varepsilon}$, is defined as the mass of liquid leaving the liquid film and entering the vapor core per unit time per unit interfacial area. The deposition rate, denoted by $\dot{m}_{dep}$, is defined as the mass of droplets leaving the vapor core per unit interfacial area per unit time and depositing in the liquid film. The entrainment fraction, denoted by E, is another important quantity used for studying entrainment. The following relation defines the entrainment fraction:

$$E = \frac{\dot{m}_{ld}}{\dot{m}_l} = 1 - \frac{\dot{m}_{lf}}{\dot{m}_l} \tag{2-1}$$

Here, $\dot{m}_{ld}$ denotes the droplet mass flow rate, $\dot{m}_l$ denotes the liquid mass flow rate and $\dot{m}_{lf}$ denotes the film mass flow rate. Figure 2 shows an illustration of important parameters.

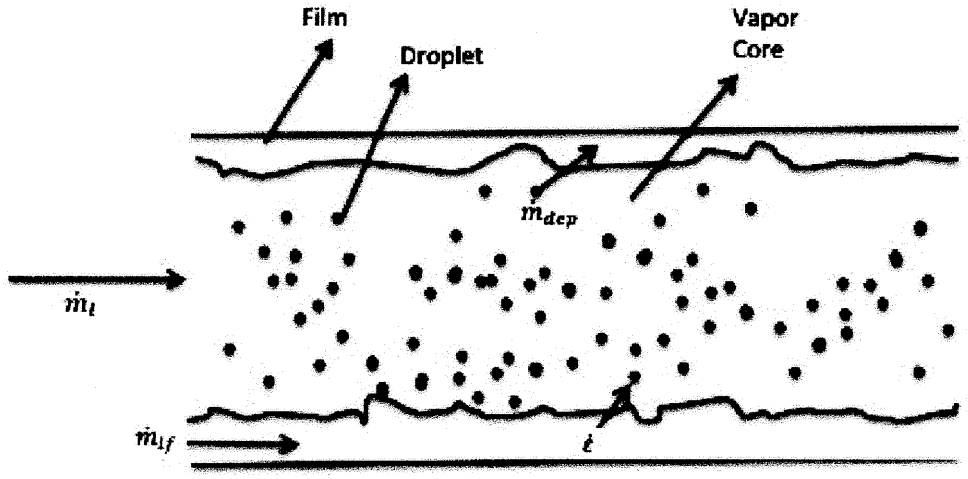

Figure 2: Entrainment Definition

2.3 Literature Review:

Kataoka and Ishii [17] and Ishii and Mishima ([10], [11]) have developed empirical correlations for predicting entrainment rates in equilibrium zones (equation 2-2) and under-entrained zone (equation 2-3). The entrainment fraction and entrance length required to reach equilibrium conditions is also predicted (equation 2-4 and equation 2-5).

$$\frac{\dot{\varepsilon}D}{\mu_l} = 6.6 * 10^{-7} * (Re_l We)^{0.925} * \left(\frac{\mu_g}{\mu_l}\right)^{0.26} \tag{2-2}$$

$$\frac{\dot{\varepsilon}D}{\mu_l} = 0.72 * 10^{-9} Re_l^{1.75} We(1 - E_\infty)^{0.25}\left(1 - \frac{E}{E_\infty}\right)^2 + 6.6 * 10^{-7}(Re_l We)^{0.925}\left(\frac{\mu_g}{\mu_l}\right)^{0.26}(1 - E)^{0.185} \tag{2-3}$$

$$E = \tanh\left(7.25 * 10^7 We^{1.25} Re_l^{0.25}\right) \tag{2-4}$$

$$z = {440DWe^{0.25}}/{Re_l^{0.5}} \tag{2-5}$$

Here $\dot{\varepsilon}$ is the entrainment rate, D is the hydraulic diameter, μ_l and μ_g are the viscosities of liquid and gaseous phase, respectively, Re_l is the liquid Reynolds number defined as $Re_l = \rho_l j_l D/\mu_l$, We is the Weber number defined as $We = \rho_g j_g^2 D(\rho_l - \rho_g)/(\sigma\rho_g)$, E is the entrainment fraction, E_∞ is the entrainment fraction at equilibrium conditions, $\rho_l$and ρ_g are the densities of liquid and gaseous phase, j_l and j_g are the liquid and gas superficial velocities and z is the entrance length. Ishii and Mishima [11] obtain satisfactory comparisons with these correlations for air-water systems in the operating ranges of $1 < p < 4atm$, $0.95cm < D < 3.2\,cm$, $370 < Re_f < 6400$ and $j_g < 100\,ms^{-1}$. These correlations were modified later by Sawant et al. ([18], [19]), but it was again observed that these correlations performed better for air-water data than steam-water data.

Lopez de Bertodano et al.[20] proposed the following correlation for entrainment rate which provides a better agreement than Kataoka and Ishii correlation for high pressure and large gas mass flow rates:

$$\frac{\dot{\varepsilon}D}{\mu_l} = \{4.47 * 10^{-7} * ((Re_{2F} - Re_{2Fc}) * We)\}^{0.925} * \left(\frac{\mu_g}{\mu_l}\right)^{0.26} \tag{2-6}$$

Here, Re_{2F} and Re_{2Fc} are the local and critical Reynolds number calculated using film thickness. It is noted that Kataoka and Ishii and Bertodano et al. use dimensionless groups for developing the correlations.

There are other correlations in literature too, which do not involve only dimensionless groups. Pan and Hanratty [21] proposed the following correlation for the prediction of equilibrium entrainment fraction:

$$\frac{E}{E_m}/1-\left(\frac{E}{E_m}\right)=k_A D j_g^{n+2} S\left(\rho_g \rho_f\right)^{0.5}/4k_d \tag{2-7}$$

Here, k_A and k_d are the atomization and deposition coefficients dependent on diameter, flow conditions and fluid properties, S is the slip ratio between the two phases, $E_m$is the maximum entrainment fraction defined by $E_m=\left(1-W_{lfc}/W_f\right)$ where $W_{lfc}$is the limiting liquid flow rate below which there is no entrainment and W_f is the total liquid flow rate. For $n=1$ in equation 2-7, k_A is dimensionless whereas k_d has units of velocity. In addition to the above, Pan and Hanratty [21] also propose a correlation for prediction of the critical gas superficial velocity j_{gc} required for the onset of entrainment:

$$j_{gc}=40\sigma^{0.5}/D^{0.5}\left(\rho_l \rho_g\right)^{0.25} \tag{2-8}$$

Dallman et al. [22] correlated the air-water data in 9.5 mm diameter test section using $k_A/4k_d=6.7*10^{-6}$ and the data in 31.8 mm diameter test section using $k_A/4k_d=6.5*10^{-5}$, however a correlation for prediction of limiting entrainment fraction was not

proposed. Other correlations have been proposed in literature for prediction of k_d ([23],[24]).

Secondi [2] recommends using Okawa et al. [24] correlation for assessment of droplet entrainment for BWR rod bundles. Secondi [2] compares the correlations developed by Okawa et al[24], Hewitt and Govan[25], Lopez de Bertodano[20], Kataoka and Ishii[17], Utsuno and Kaminga[26] and Dallman[22] for air-water and steam-water data and find that the correlation of Okawa et al.[24] performs much better than any other correlations for entrainment rate calculations for both air-water and steam-water annular flows (see Table 1). Table 1 shows the ratio of experimentally measured values for a wide range of datasets to the predicted values by correlations as described by Secondi [2].

Table 1: Entrainment Rate Comparison (Experimentally Measured/Predicted Value Ratio) for Different Correlations as described by Secondi[2]

	Steam-Water Mean Value	Steam-Water Standard Deviation	Air-Water Mean Value	Air-Water Standard Deviation
Okawa	0.9182	0.3815	0.7737	0.3209
Govan	0.8501	0.5179	0.5320	0.2741
De Bertonado	2.6751	3.3867	1.9786	1.2123
Kataoka	1.6693	2.5501	2.5155	1.4221
Utsuno	1.0842	0.3731	6.9212	27.0154
Dallman	11.7340	17.9194	1.4481	1.1630

Okawa et al. [24] correlation for estimation of equilibrium entrainment fraction for high pressure involves solving the following equations:

$$k_d\sqrt{\frac{\rho_g D}{\sigma}} = 0.0632\left(\frac{C}{\rho_g}\right)^{-.5} \tag{2-9}$$

$$C \approx \frac{E\rho_l j_l}{j_g} \tag{2-10}$$

$$\frac{Ek_d j_l}{j_g} = k_e \pi_e^n \tag{2-11}$$

$$\pi_e = f_i \rho_g j_g^2 / (\frac{\sigma}{\delta}) \tag{2-12}$$

Here, k_d is the deposition coefficient, C is the droplet concentration in core in kg/m^3, D is the equivalent diameter, E is the equilibrium entrainment fraction, ρ_l and ρ_g are liquid and vapor densities, σ is the surface tension, t_f is the liquid film thickness, f_i is the interfacial friction factor. The interfacial friction factor can be estimated by Wallis correlation [27] as follows:

$$f_i = 0.005(1 + 300\frac{t_f}{D}) \tag{2-13}$$

The parameters k_e and n in equation 2-11 can be represented by the following relation:

$$\begin{cases} k_e = 3.1\times10^{-2}\ m/s\ \ and\ n = 2.3\ for\ \pi_e < 0.0675 \\ k_e = 1.6\times10^{-3}\ m/s\ \ and\ n = 1.2\ for\ 0.0675 < \pi_e < 0.295 \\ k_e = 6.8\times10^{-4}\ m/s\ \ and\ n = 0.5\ for\ \pi_e > 0.295 \end{cases} \tag{2-14}$$

This correlation will be used later for macroscopic comparisons of results from simulations.

2.4 Computational Modelling Efforts:

It is common to model annular flows using multi-field models ([28], [29]). The multi-field models basically involve solving the Navier Stokes equation for each phase separately. The interaction between the phases is taken into account by adding mass, momentum and energy transfer exchange terms in the conservation equations. These exchange terms are modelled using empirical correlations. The disadvantage of using this approach is that the correlations have a limited database and are based on oversimplifying assumptions related to interface geometries and hence are inaccurate.

Hizoum et al [30] at GE use COBRAG code for development of droplet deposition and entrainment models. COBRAG is based on three fluid-multi film model and the models are validated using in-house high pressure steam water data for individual channels and 8x8 BWR-type fuel bundles.

Michta et al. [31] have used OpenFOAM solver with multi-fluid formulation to develop models for bubbly flows. The code CATHARE has also been used by Yao and Morel [32] to give an insight into bubbly flow physics based on multi-fluid formulation.

Damsohn and Prasser [33] studied the enhancement of droplet deposition (and hence dryout reduction) in BWR assemblies using functional spacers via experimental and

computational means. In their CFD model, they employ a Eulerian-Lagrangian approach to model droplet deposition. The RANS-based Eulerian approach is used to obtain a converged vapor field and then droplets are injected and followed in a Lagrangian manner until they get deposited or fragmented into smaller droplets.

Lahey[34] describes the use of direct numerical simulation to provide high quality data for multiphase flows. Lahey[34] also describes the use of this DNS data for providing closure laws for existing multi-fluid models. Rodriguez [35] performed a direct numerical simulation with an interface tracking approach using PHASTA – IC code to model annular flow and is able to capture the physics of the problem such as ligament formation and droplet shearing by simulating a portion of the domain. However, the domain used in this work was only $1/8^{th}$ of the mean wavelength in stream-wise direction, which may introduce geometric distortions in the solution.

3. INTERFACE TRACKING METHODS

In this section, an overview of interface tracking methods is provided. Several interface tracking techniques have been presented in the literature to capture interfaces. Lakehal et al.[36] and Tryggvason et al. [37] provide a good review of the interface tracking techniques that have been frequently employed.

As mentioned in the previous section, solving the conservation equations for multiphase flows has proven to be a very challenging problem. Most of the existing modeling techniques employ use of empirical models and hence are only applicable to situations where resolving the details of interface geometry and interfacial exchanges is not important. Interface tracking methods eliminate the usage of such oversimplifying assumptions and track interface evolution from "first principles".

The interface tracking methods typically involve use of "one-fluid" formulation unlike most other modeling techniques which involve usage of "multi-fluid" formulation as described in the section above. The one fluid formulation treats the entire fluid as a single field with varying properties across different phases. This leads to the presence of additional source terms (such as surface tension and phase change) at the interface. The interface tracking methods can be categorized into a number of different categories such as level set methods, volume of fluid methods and front tracking methods, as described by Lakehal et al.[36] and Tryggvason et al. [37].

In the following subsections, a brief review of volume of fluid methods and level set methods is provided and a description of one-fluid formulation is also provided. The limitations of VOF and level set methods are also discussed.

3.1 One Fluid Formulation:

In order to mathematically define multiphase flows as one-fluid, the concept of a component indicator function is used. The component indicator function χ_k for phase k is defined such that $\chi_k = 1$ for phase k and $\chi_k = 0$ otherwise. Since χ_k is a property moving with the flow, its material derivative is 0 for no phase change (Drew and Passman [38]). This gives the following advection equation for χ_k which is known as the topological equation:

$$\frac{D\chi_k}{Dt} = \frac{\partial \chi_k}{\partial t} + \boldsymbol{u}.\nabla\chi_k = 0 \tag{3-1}$$

Note that the above equation is a weak formulation as χ_k is not continuous across the interface and hence not differentiable. Now, in the absence of mass transfer, the continuity equation for each of two non-miscible, non-reacting phases can be described by the following equations (Note the subscript 'L' and 'G' represents each phase):

$$\frac{\partial \rho_L}{\partial t} + \boldsymbol{u}.\nabla\rho_L = 0 \tag{3-2}$$

$$\frac{\partial \rho_G}{\partial t} + \boldsymbol{u}.\nabla\rho_G = 0 \tag{3-3}$$

Multiplying equation 3-2 by χ_L and equation 3-3 by (1-χ_L), and adding the two equations, the following equation can be obtained:

$$\frac{\partial \rho}{\partial t} + \nabla.(\rho \boldsymbol{u}) = 0 \tag{3-4}$$

with

$$\rho = \rho_G + (\rho_L - \rho_G)\chi_L \tag{3-5}$$

Assuming that the two phases are incompressible, and using equation 3-1, equation 3-4 can be reduced to:

$$\nabla.\boldsymbol{u} = 0 \tag{3-6}$$

Note that this result is different from $\nabla.(\rho \boldsymbol{u}) = 0$ and hence is important as certain Navier Stokes solvers use this equation which is clearly not compatible with equation 3-6.

The Navier Stokes (momentum) equation and energy equation for the "one-fluid" formulation can be written as:

$$\frac{\partial \rho \boldsymbol{u}}{\partial t} + \nabla.(\rho \boldsymbol{u}\boldsymbol{u}) = -\nabla p + \nabla.\tau + \rho \boldsymbol{g} + \gamma \nabla.\varphi \tag{3-7}$$

$$\frac{\partial \rho E}{\partial t} + \nabla.(\rho E \boldsymbol{u}) = \nabla.(k\nabla T) + (-pI + \tau + \gamma\varphi):\nabla \boldsymbol{u} \tag{3-8}$$

Here g stands for acceleration due to gravity, p for the pressure, E for the internal energy, T for the temperature, k for the heat conductivity, $\tau = \mu(\nabla u + \nabla u^T)$ denotes the viscous stress tensor, with μ representing the dynamic viscosity, and φ is the capillary stress, with γ being the coefficient controlling the strength of capillary forces. In these equations, material properties depend locally on the phase indicator function determined by the use of topological equation (equation 3-1) and are denoted as

$$\zeta = \zeta_g + (\zeta_g - \zeta_l)\chi_L \tag{3-9}$$

It is to be noted that the above relation does not necessarily hold for viscosity and can only be used as model. In order to ensure continuity across interface, the velocity and shear stress are the only criteria that should remain continuous and the viscosity does not come into picture.

Physically, the capillary term φ in the above system of equations represents the energy concentrated at a diffuse interface because of the prevailing density or concentration field gradients (Anderson et al.[39]). Chella and Vinals [40] have shown that in the limit of smoothly curved, thin interfaces, and when the interface motion is slow compared with the local relaxation time of χ_L, the capillary source term appearing in equations 3-7 and 3-8 can be approximated by

$$\gamma\nabla.\boldsymbol{\varphi} \approx -|\nabla\chi|^2 K\kappa\mathbf{n} \tag{3-10}$$

where n denoted the unit vector normal to the interface, K is a positive constant, and κ represents the local curvature represented by the following relation:

$$\kappa = -\nabla.\mathbf{n} = -\nabla.\left(\frac{\nabla\chi}{|\nabla\chi|}\right) \tag{3-11}$$

Brackbill et al. [41] showed that by integrating this equation over interfacial area it is possible to get:

$$\gamma\nabla.\boldsymbol{\varphi} \approx \int \sigma\kappa\delta(x - x_f)\mathbf{n}ds \tag{3-12}$$

where σ is the surface tension, assumed to be constant across the entire thickness of the interfacial sub-layer, and $\delta(x - x_f)$ represents a Dirac pulse with x_f being the instantaneous location of the interface. Physically, the surface tension represents the excess capillary energy concentrated at the surface per unit surface area caused by the variation in composition field across the interfacial sub-layer. The above model is also called Continuous Surface Model (CSF). The CSF model is robust, simple and very easy to implement. A number of validation exercises for CSF based models have been performed by Meier et al. [42].

In the above section, a brief overview of the general one-fluid formulation was provided. In the following sections, the application of one fluid formulation to the level set and volume of fluid methods will be discussed.

3.2 Volume of Fluid Method:

This approach relies on the definition of a liquid volume fraction field given by the following equation:

$$F_{ij} = \frac{1}{V}\left(\int_{cell\ volume} \chi(x,t)dV\right) \tag{3-13}$$

F_{ij} denotes the liquid characteristic function such that $F_{ij} = 1$ for a liquid fraction of 1 inside the cell volume, $F_{ij} = 0$ for a liquid fraction of 0 (gas fraction of 1) inside cell volume and $0 \leq F_{ij} \leq 1$.

The main motivation behind using volume of fluid methods is that they conserve mass. If the topological equation for interface (equation 3-1) is solely used, it leads to a reduction in mass of liquid due to the numerical errors involved in advecting the phase distribution function. Hence, volume of fluid methods do not solely amount to advection of the topological equation, but they also involve the advection of fluid characteristic function F_{ij}. The advection of F_{ij} is a challenging task as they are discontinuous.

In terms of implementation, VOF methods involve advection of fluid characteristic functions F_{ij} instead of the phase indicator function (in equation 3-1). The interface geometry χ is instead reconstructed using special reconstruction algorithms from local volume fraction data and interface information. Reconstruction schemes typically involve use of vertical or horizontal lines in each cell to reconstruct interfaces or PLIC (piecewise linear interface construction) methods (Rider and Kothe [43]).

When interface geometry plays a crucial role and it is necessary to resolve the interface and track its evolution, this technique is not particularly suited as it involves reconstruction algorithms. For such cases, the level set methods can be used and they are described below.

3.3 Level Set Method:

The level set methods involve advecting a marker function ϕ to advect an interface. The level set function has a value of 0 at interface between the two fluids. At any given location inside the domain, the level set function is considered to be signed a distance from the interface. This means that ϕ is 0 for the interface, negative for one-fluid and positive for the other fluid. This method provides a clear distinction between two phases and provides an easy mode for dealing with problems that involve merging of interfaces, and computing interfacial curvature.

Mathematically, the equation for advection of level set can be represented by the following equation:

$$\frac{D\phi}{Dt} = \frac{\partial \phi}{\partial t} + \boldsymbol{u}.\nabla\phi = 0 \qquad (3\text{-}14)$$

It is essential to relate the composition field as described by equation 1 with the level set function in this formulation. The composition field is related to level set function using the following relation:

$$\chi_k = H(\phi) \tag{3-15}$$

where $H(\phi)$ is the Heaviside function represented by the following function:

$$H(\phi) = \begin{cases} 1, & \phi < 0 \\ 0, & \phi > 0 \end{cases} \tag{3-16}$$

It can be noted here that the F_{ij} described in equation 3-13 for VOF method is directly linked to ϕ by the following equation:

$$F_{ij} = \frac{1}{V} \int H[\phi_{ij}]\, dV \tag{3-17}$$

It was discussed in the earlier sections that one fluid formulation has a disadvantage in the fact that is non-differentiable at the interface as the properties are discontinuous. The same applies to level set methods. This could create a severe limitation in the implementation of level set methods in numerical solvers that involve solution of Poisson equation for pressure (such as Fedkiew et al. [44]) and drastic property differences in the two phases. In order to effectively eliminate this discontinuity in properties, the interfacial thickness is relaxed and the properties are allowed to vary in a differentiable manner over the relaxed thickness. This is known as interface relaxation and implemented by using a modified Heaviside function, as shown in equation 3-18 and 3-19 and as described by (Sussman and Smereka [45]).

$$\overline{H}(\phi) = \begin{cases} 0, & \phi < -\delta \\ 1 + \frac{\phi}{\delta} + \frac{1}{\pi}\sin\left(\frac{\pi\phi}{\delta}\right), & |\phi| \leq \delta \\ 1, & \phi > \delta \end{cases} \quad (3\text{-}18)$$

$$\zeta(\phi, t) = \zeta_G + (\zeta_L - \zeta_G)\overline{H}(\phi) \quad (3\text{-}19)$$

Here, the Heaviside function $\overline{H}(\phi)$ is typically used to smooth the physical properties over a distance 2δ which typically covers 1 to 2 cells. This effectively renders the physical properties described by equation 3-19 differentiable.

There are two kinds of numerical errors that arise in level set methods. These errors are described as follows:

- Firstly, the use of interfacial thickness relaxation and the usage of a modified Heaviside function as described by equation 3-18 does not assure mass conservation. To take this error into account, a global volume correction algorithm as suggested by Lakehal et al [36] can be employed. This method adds the error in volume at every given time step in a time-relaxed manner such that the total volume remains constant.

- Secondly, the computational errors involved in the use of advection equation for level set function (equation 3-14) tends to deform the level set contours and an additional operation is required to re-distance the level set function such that it preserves the necessary condition of $|\nabla\phi| = 1$ around the interface. This error is

termed as interface smearing and a number of re-distancing algorithms have been proposed by different researchers for taking this into account.

As a final note to this section, the use of level set methods is preferred over volume of fluid methods for entrainment modeling as the interfacial information and evolution is very important for stratified wavy and annular flows, and for extracting interfacial features.

4. TURBULENCE MODELING

Turbulent flows are highly chaotic, rotational and dissipative. Unlike laminar flows, the numerical treatment of turbulent flows is challenging due to their rapid time fluctuations. Furthermore, if the two phase flow treatment is also included in the modeling effort, the complexity of the problem greatly increases. In the following subsection, a brief description of the nature of turbulence and common modeling techniques is provided. In addition to this, an overview of the Large Eddy & Interface Simulation (LEIS) method used in this work for modeling stratified and annular flows is also provided.

4.1 Nature of Turbulence:

Turbulent flows have been typically characterized as a spectrum of velocity fluctuations and eddies contained within a flow. The eddies refer to coherent patterns of velocity, vorticity and pressure. Turbulent flows may be viewed as a superposition of eddies containing energy over a wide range of length scales and hence these eddies constitute an energy spectrum. This energy can freely "cascade" from large eddies (higher length scales) to small eddies (smaller length scales). Generally, the length scales l are represented by wave number denoted by k and given by $k = 2\pi/l$.

The scales in the energy cascade are generally uncontrollable and highly non-symmetric. Nevertheless, based on their length scales these eddies can be divided into three categories as shown in Figure 3. These regimes are further described as follows:

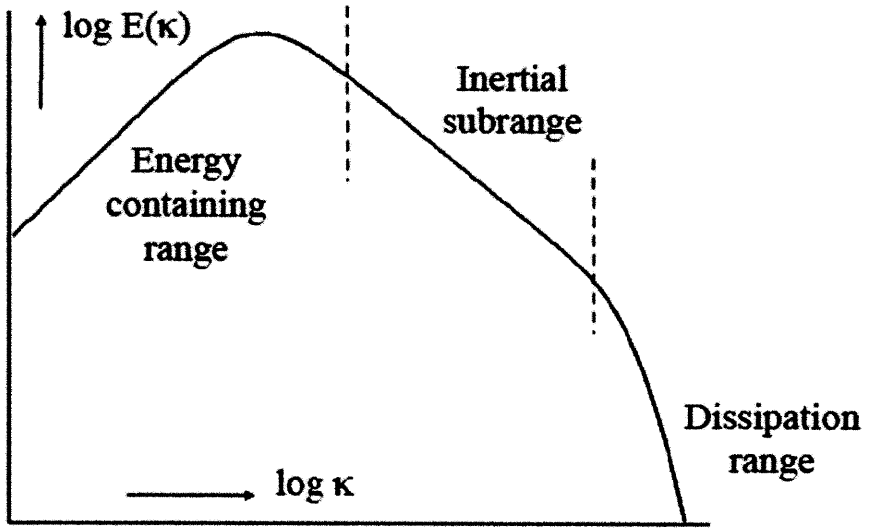

Figure 3: Typical high-Re turbulent spectrum

- Energy Containing Range: This contains the largest scales in the energy spectrum. The eddies formed within this range gain energy from the mean flow and from each other. Hence, this regime contains energy producing eddies within a turbulent spectrum. They have large velocity fluctuations, are low in frequency and are highly anisotropic. The maximum length of these scales is constrained by the characteristic length of the apparatus. Since they can have a high degree of anisotropy associated with them and are dependent on the geometry of the problem as well, it is not convenient to develop with a universal model that could accurately describe them.
- Inertial Sub-Range: This range contains the intermediate scales between the largest and the smallest scales. The scales in this range are called Taylor micro-scales. The eddies in this range simply pass down energy from the larger scales in energy

containing range to the smaller scales in energy dissipation range. They are neither energy producing nor dissipative.

- Dissipation Range: This range contains the smallest scales in the turbulent spectrum. These scales are also referred to as Kolmogorov Scales. These scales are responsible for viscous dissipation. In this range, the energy input from nonlinear interactions arising due to non-homogeneous and anisotropic large scale energy containing eddies and the energy drain from viscous dissipation is in exact balance. The small scales have high frequency, and tend to be locally isotropic and homogeneous. Since these scales are isotropic, they are amenable to being represented by a universal model which describes their contribution to turbulence spectrum and this can be widely used in turbulence modeling techniques as will be seen in the sections to follow. By using simple dimensional analysis, the Kolmogorov length and time scales can be estimated by equation 4-1 and equation 4-2.

$$\eta = \left(\frac{\nu^3}{\epsilon}\right)^{\frac{1}{4}} \tag{4-1}$$

$$\tau_\eta = \left(\frac{\nu}{\epsilon}\right)^{\frac{1}{2}} \tag{4-2}$$

Here, ν is the kinematic viscosity, ϵ is the average rate of dissipation of turbulence, η and τ_η are Kolmogorov length and time scales respectively. Note that η and τ_η give an idea of the smallest length and time scales in the problem and this is very important for CFD modeling approaches as it has direct implications on grid resolution and numerical errors.

4.2 Computational Modelling Approaches:

As discussed in the previous section, turbulence involves eddies with a large range of length and time scales. The common methods that are used for treatment of turbulence are direct numerical simulations (DNS), large eddy simulations (LES), Reynolds-Averaged Navier Stokes Simulations (RANS) and other hybrid methods. In this section, a brief overview of these methods will be provided. Pope[46] provides a good review of these computational modeling approaches.

4.2.1 Direct Numerical Simulation (DNS):

The DNS method is based on direct solution of the Navier Stokes equations and energy equation (if heat transfer is present). DNS methods can be thought of as exact solutions to Navier Stokes equations. DNS resolves everything in the flow down to the Kolmogorov scales. Assuming that the equations to be solved represent the physics of the problem exactly, DNS in principle does not require experimental validation. Instead, it can be used for providing data in cases where experimental measurements are not available. The errors accumulated in DNS only correspond to errors that arise due to numerical schemes and sensitivity to perturbation of initial conditions. This is the biggest advantage of DNS methods.

For problems involving flows with high Reynolds number, the use of DNS is not advisable. Because DNS involves resolving all scales within the flow, computational costs required for moderate to high Reynolds number flows is very high. As the Reynolds number increases, the frequency of smaller turbulent scales increases and hence a larger number of grid points is needed to completely resolve it. It can be shown that the number

of grid points required to completely resolve a turbulent flow are approximately equal to $Re^{\frac{9}{4}}$ [46]. In addition to the decrease in length scale to resolve Kolmogorov scale, the minimum time scale needed to resolve flow characteristics also decreases with increase in Reynolds number. This has a direct implication on the total computational time required for simulating a given amount of time. The disadvantage of having high computational cost is that a parameter sensitivity study cannot be generally carried out.

4.2.2 Reynolds Averaged Navier Stokes (RANS):

RANS are time-averaged equations, which provide information about the mean flow and some statistics about the fluctuation field. This method typically involves decomposition of an instantaneous quantity into time averaged and fluctuating quantities. These simulations usually require a closure model for modeling the turbulent stresses. Some of the closure models that exist in literature are eddy viscosity models, turbulent kinetic energy model, $k-\epsilon$ models and $k-\omega$ models.

The main advantages of these methods are that they have less strict time/grid requirement and can be used to simulate large scale engineering problems with flows involving high Reynolds numbers. However, these methods have a major disadvantage in the fact that they only provide information of the mean flow. The use of closure models automatically removes the robust physics that can be seen in DNS/LES techniques. For simple flows, these models can indeed provide acceptable accuracy. However, for complex flows, the accuracy of these models cannot be trusted. These methods need to be validated with experiments and their applicability is only limited to the validated parameter space. However, these methods can be used to provide good initial guesses for complex

problems and then these guesses can be used to obtain finer solution using DNS/LES methods.

4.2.3 Large Eddy Simulation (LES):

Large Eddy Simulation (LES) methods focus on capturing the large scale eddies. These methods typically resolve down to an eddy size located inside the inertial sub-range. The smallest eddies are not resolved, but their effects are modeled. As was discussed in section 2.1, the eddies in the dissipative range are isotropic and universal across every flow problem, thus they can be conveniently modeled using universal models. Figure 4 gives an idea of the scales resolved by LES.

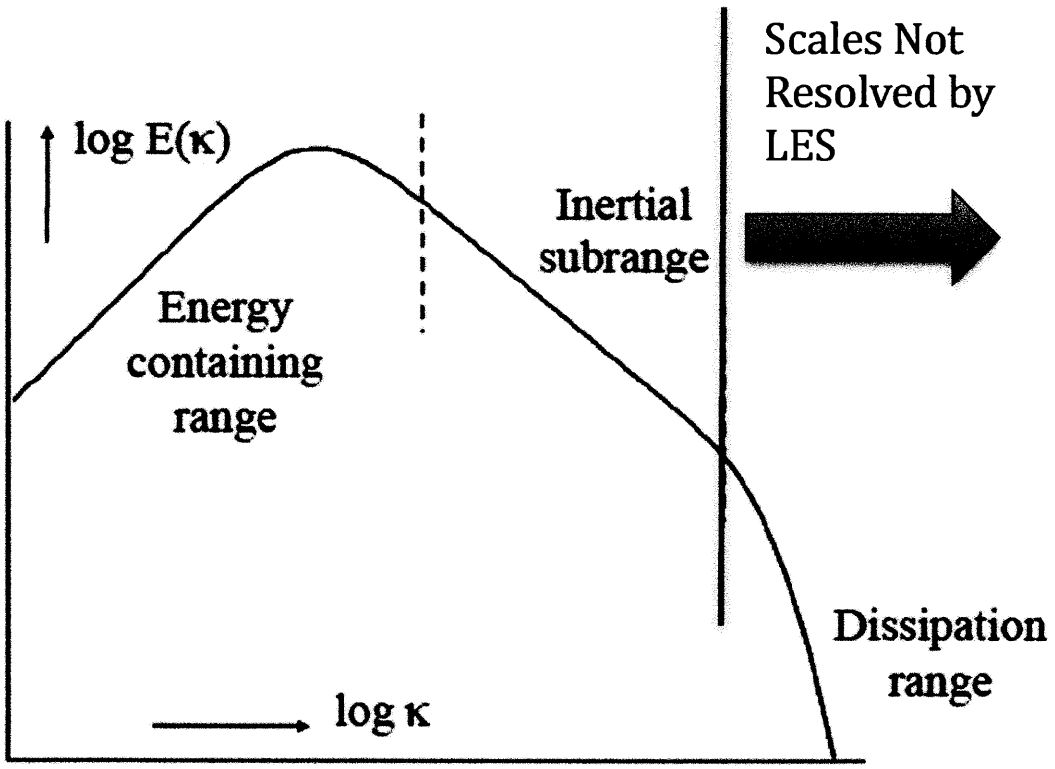

Figure 4: Scales Captured by LES

LES has the following three conceptual steps:

a) Design Filter: The use of design filter in LES removes scales in the dissipative (Kolmogorov) range. For any given quantity *u(x,t)*, the design filter implementation is given by the following relation:

$$\bar{u}(x,t) = \int G(x-x')u(x',t)d^3x' \tag{4-3}$$

Here *G(x)* is the design filter and can be Gaussian, box, spectral cutoff etc. $\bar{u}(x,t)$ denotes the filtered field.

b) Filtered Navier Stokes and Continuity Equation: This step involves decomposing velocity and pressure fields into filtered and sub-grid (unresolved) fields. Upon carrying out this step, the following equations are obtained:

$$\frac{\partial \overline{u_i}}{\partial t} + \bar{u}_j \frac{\partial \overline{u_i}}{\partial x_j} = -\frac{1}{\rho}\frac{\partial \bar{p}}{\partial x_j} + \frac{\nu \partial^2 \overline{u_i}}{\partial x_j^2} - \frac{\partial \tau_{ij}}{\partial x_j} \tag{4-4}$$

$$\tau_{ij} = \overline{u_i u_j} - \bar{u}_i \bar{u}_j \tag{4-5}$$

$$\frac{\partial \bar{u}_i}{\partial x_i} = 0 \tag{4-6}$$

c) Closure Models: the term τ_{ij} appears in the equations. This term takes into account the dynamics of sub-grid scales and needs to be modeled. Since small scales are not resolved, viscous dissipation is not resolved and needs to be modeled correctly. There are a number of models that can be used for modeling

these smaller scales but the most commonly used model is Smagorinsky's model which will be discussed in the next section.

LES has a major advantage as it is less expensive than DNS but much more accurate than RANS. It only requires modeling small scales. However, it has few limitations. Even though LES is less expensive than DNS, it is still computationally onerous for engineering flows. LES is extremely sensitive to initial conditions. However, for high Reynolds number flows and in cases where computational costs are important limiting criteria, LES is a convenient choice.

4.3 Large Eddy Interface Simulation (LEIS):

In chapter 3, the need for interface tracking methods to accurately track multiphase flows was emphasized. If the multiphase flows are coupled with turbulence as well, computational approaches to deal with such problems become extremely challenging. In such kind of problems, the best strategy would be to use interface tracking with a turbulence modeling technique that is low on computational costs but reasonably accurate. The use of DNS is not possible for most problems of practical interest, as the computational costs associated with it are extremely high. The use of RANS method puts a severe limitation on the accuracy of results obtained for interfacial phenomena and even turbulence. This automatically renders LES as the ideal practical approach for modeling problems involving multiphase flows and interface tracking. The combination of these approaches is termed as Large Eddy Interface Simulation (LEIS) and it is described in this section.

A brief overview of LEIS method has been provided by Lakehal [47]. The method involves filtering continuity and Navier Stokes equations obtained for one-fluid formulation (equation 3-1 and equation 3-7). The difference between single incompressible phase flows and multiphase flows lies in the fact that the convolution operator (as defined by equation 4-3) must take into account density and viscosity variations within the fluid. It is noted that if the multiphase system is modeled as "one-fluid", it has a variation in density and viscosity. Upon filtering the one-fluid equations, the system of equations obtained is as follows:

$$\frac{\partial \overline{\chi}}{\partial t} + \frac{\partial \overline{u}_j \overline{\chi}}{\partial x_j} = 0 \tag{4-7}$$

$$\frac{\partial \overline{\rho}}{\partial t} + \frac{\partial \overline{u}_j \overline{\rho}}{\partial x_j} = 0 \tag{4-8}$$

$$\frac{\partial}{\partial t}(\bar{\rho}\bar{u}_i) + \frac{\partial}{\partial x_j}(\bar{\rho}\bar{u}_i\bar{u}_j) = \nabla.(\overline{\Pi} - \tau) - (\nabla.\bar{n})\gamma\bar{n} + \Sigma R + \bar{\rho}g \tag{4-9}$$

In the above equation, τ is the sub-grid scale stress tensor, which needs to be modeled, and R is the sum of convolution-induced errors. R has been shown to be negligible by Liovic and Lakehal [48].

In order to model the sub-grid scale stress tensor τ_{ij}, Reboux et al. [49] have shown that the most important factor to consider is to account for decay in turbulence near interface boundary layers in a similar manner as in wall flows. Within the eddy viscosity framework,

$$\tau_{ij} = 2\nu_t S_{ij} + \frac{\delta_{ij}\tau_{kk}}{3} \tag{4-10}$$

$$\nu_t = f_\mu^{int}(C_s\Delta)^2\sqrt{2\overline{S_{ij}}\,\overline{S_{ij}}} \tag{4-11}$$

Here, the length scale is based on the mesh Δ and C_s is the model coefficient typically equal to 0.1, and S_{ij} is the strain rate, f_μ^{int} is the turbulence damping function near the walls. Reboux et al. [49] provide a description of models used for prediction of damping function.

5. TransAT – Code Description and Benchmark Cases

5.1 TransAT• multiphase flow software:

The CFD/CMFD code TransAT© developed at ASCOMP Switzerland is a multi-scale, multi-physics, conservative finite-volume code which solves the single- and multi-fluid Navier-Stokes equations. TransAT exists in two versions: Single Block (TransAT-SB) and Multi-block (TransAT-MB). While TransAT-SB is parallelized using the OpenMP-Protocol on PC's and laptops, TransAT-MB uses MPI and domain decomposition methods to run on non-shared memory supercomputer clusters. The code uses structured multi-block meshes, with the grids having two layers of ghost cells where information from neighboring blocks is received. An MPI (Message Passing Interface) parallel based algorithm is used in connection with multi-blocking. The grid arrangement is collocated and thus can handle curvilinear skewed grids easily. The solver is pressure based (Projection Type), corrected using the Karki-Patankar technique for low-Mach number compressible flows. High-order time marching and convection schemes can be employed; up to 3rd order Monotone schemes in space and 5th order in time. Turbulent flows can be treated in three ways: RANS statistical models, Scale Resolving Approaches like LES and its DES and VLES variants, and pure DNS. LES and DNS are built within the explicit version of the code, with their proper routines for pressure coupling, boundary conditions, diffusive fluxes and near-wall stress integration. TransAT uses high-order schemes for convection and diffusion processes in the linearized, discretized transport equations. Briefly, the schemes employed for convection in all equations are: HLPA (2nd order), CENTRAL (2nd order), QUICK (3rd order), SOUCUP (2nd order),

HYBRID & UPWIND (1st order), TVD-based Schemes (2nd order). The schemes employed for time marching are EULER (1st and 2nd order), TLFI (2nd order), Runge-Kutta (2nd to 5th order). The schemes employed for pressure-velocity coupling are: SIP, GMRES, GMG & AMG, augmented using the parallel PETSc solver library. For large-scale problems, TransAT© is parallelized using MPI.

5.2 Benchmark Cases:

5.2.1 Two Dimensional Wavy Liquid Film Falling Under Gravity:

In order to benchmark TransAT for multiphase modelling and interface tracking capabilities, a benchmark case of two dimensional wavy liquid film falling under gravity is used. It is noted that the velocity shear at the interface between the liquid phase and the gaseous phase deforms the surface. The physics concerning this phenomenon is similar to droplet entrainment as it involves large interfacial deformations, thus making it an ideal benchmark case for investigation of multiphase modelling and interface tracking capabilities.

A detailed study for the falling liquid film has been carried by Nave [5]. A similar study is performed with TransAT. The computational data are compared with experiments of Nosoko et al. [50]. In order to effectively compare the codes, similar dimensionless groups for describing the properties, interface wavelengths and Reynolds numbers are used [50]:

$$N_f = \frac{\rho^3 \nu^4 g}{\sigma^3} \tag{5-1}$$

$$N_{hp} = h_{peak}\left(\frac{\nu^2}{g}\right)^{-\frac{1}{3}} \tag{5-2}$$

$$N_{\lambda} = \lambda_s\left(\frac{\nu^2}{g}\right)^{-\frac{1}{3}} \tag{5-3}$$

Here N_f, N_{hp} and N_{λ} are the non-dimensional fluid property group, non-dimensional peak height (amplitude) and non-dimensional wavelength, respectively, ρ is the density of liquid, ν is the kinematic viscosity of liquid, g is the acceleration due to gravity, h_{peak} is the peak height and λ_s is the wavelength of the waves at steady state observed in experiments. The velocity scale is defined by

$$V = (\nu g)^{1/3} \tag{5-4}$$

The Reynolds number is calculated based on undisturbed film thickness h_0 and is given by:

$$Re = \frac{Vh_0}{\nu} \tag{5-5}$$

Nosoko et al. [50] also propose the following empirical correlation for predicting the amplitude of the observed wavelengths for laminar two dimensional falling wavy liquid films:

$$N_{hp} = 0.49N_f^{0.044}N_{\lambda}^{0.39}Re^{0.46} \tag{5-6}$$

Figure 5 shows typical wave profiles obtained by TransAT and schematic of profile observed by Nosoko et al. [50]. Roll waves and capillary waves can be clearly seen in each of these cases. Table 2 shows the simulation parameters used for this benchmark.

The simulations with TransAT were run for a 56x256 grid with 56 points in the wall normal direction and 256 points in the streamwise direction. The level set equation was advected using the 3rd order Quick scheme, combined with the 3rd order WENO scheme for its re-initialization. The maximum and minimum CFL limits used were 1.3 and 0.8. The CFL number C is defined as $C = (u\Delta t)/\Delta x$, where u is the velocity, Δt is the time-step and Δx is the grid size. In CFD simulations, CFL number defines an upper limit for the time-step needed to accurately resolve a wave moving with speed u over a given grid spacing Δx.

The boundary conditions were set to periodic in the streamwise direction and no-slip in the wall normal direction. The convergence was achieved when the wave amplitudes achieved steady state.

Table 3 shows the computation matrix and the results obtained from the simulations. The Reynolds number based on initial film thickness, liquid property group and the dimensionless wavelength is specified and the dimensionless peak heights are computed from the simulation and compared with the experimental correlation (equation 5-6). All physical properties, except surface tension, are the same as that of water for liquid and air for gaseous phase at atmospheric pressure. This fixes the velocity scale (as defined by equation 5-4) and hence the initial (undisturbed) film thickness is calculated based on the Reynolds number to be used. The surface tension is varied to obtain different N_f.

The Reynolds number corresponds to laminar flow regime. The dimensionless peak height group from the experimental correlation of Nosoko et al. [50] and the code TransAT is computed and compared. It can be observed from Table 3 that TransAT gives relatively small deviations from the correlations of Nosoko et al. [50].

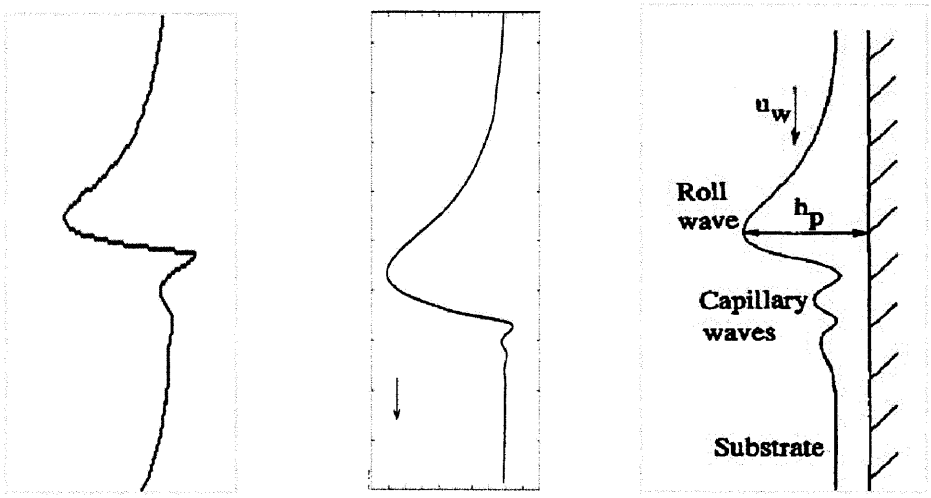

Figure 5: Typical wave profile obtained with (a) TransAT, (b) Nave [5] for case 4 in Table 1; (c) Qualitative nature of wave profile described by Nosoko et al. [50]

Table 2: Simulation Parameters for Wavy Falling Liquid Films

Solution Scheme	Implicit
Time step	10^{-6} s
Surface Tension Formulation	Implicit
CFL limits	0.8-1.3
Level Set advection Scheme	WENO 4th order
Grid Aspect Ratio	25:1

Table 3: Dimensionless Peak Heights calculated with TransAT

Serial No.	Re	N_f x 10^{-12}	N_λ	N_{hp} from Nosoko et al.	N_{hp} (TransAT with implicit surface tension formulation)	N_{hp} (TransAT with explicit surface tension formulation)
1	20	43.88	626.2	8.388	7.821	7.227
2	40	0.1614	689.4	9.360	9.247	Wave Breaks
3	50	0.2018	742.6	10.783	9.371	n/a
4	103	0.0520	994.9	15.876	13.284	n/a
5	103	0.4100	994.9	17.386	17.013	16.683

Another feature of the code is the implementation of an implicit surface tension formulation, which allows use of fewer time steps, thus speeding up the simulation. The implicit formulation also improves accuracy as seen by a comparison with the explicit formulation for the same grid sizes (see Table 1, two rightmost columns). The explicit surface tension formulation in space and time for capillary flows imposes a restriction on minimum grid size and time step. However, the implicit surface tension formulation is stronger as it does not lead to such a restriction. In the given numerical limits, it was found that the implicit surface tension formulation was more accurate than the explicit one.

5.2.2 Large Eddy Simulation of Single Phase Channel Flow:

In order to assess TransAT's predictive capabilities as to turbulence, a benchmark case of single phase flow in a horizontal channel is used. Numerical simulations for this case have been carried out by a number of researchers ([51], [52]). For the purpose of comparison, the LES simulation is performed for a bulk Reynolds number of 6300 (corresponding to a shear Reynolds number $Re_\tau = 400$) and compared with the DNS of Krogstad et al. [51]. The computational domain used is $4\pi h * 2\pi h * 2h$ and the grid size is 111 x 92 x 92 (streamwise x spanwise x wall normal direction). Here, h is the channel half width. The boundary conditions are periodic in the streamwise and spanwise directions and no slip in the wall normal direction.

The grid was created using the grid generator TransATMesh included in TransAT. The grid is staggered, Cartesian with uniform cell dimensions in streamwise and spanwise direction, and refined near the wall with a maximum and minimum ratio of 3 and 1.1 between the cell dimensions (in the wall normal direction). For the purpose of computation, an explicit Range-Kutta 3rd order time scheme is used. The maximum and minimum CFL limits are 0.1 and 0.3. The turbulent kinetic energy of the liquid in channel was used as an indicator of convergence. The convergence is achieved when the turbulent kinetic energy achieves a statistically steady state.

The results for normalized velocities and normalized Reynolds stress components are shown in Figure 6. The sub-grid scale model used in these LES is based on the eddy viscosity kernel by reference to Smagorinsky, combined with near-wall damping of turbulence using a harmonic mean between the Prandtl mixing-length defined by (ky), where k is the von Karman constant

and y is the wall distance, and ($C_s\Delta$), where C_s is the SGS model constant and Δ is the filter width. The quantities plotted in the figure below are scaled using the frictional velocity $u_\tau = \sqrt{\tau_w/\rho}$, and plotted versus either the viscous length scale $y^+ = \frac{u_\tau y}{\nu}$, or y/h, where h is the half channel width. It is seen that a reasonable agreement between LES and DNS is achieved; noting the selected shear Reynolds number is actually rather high for the computational grid.

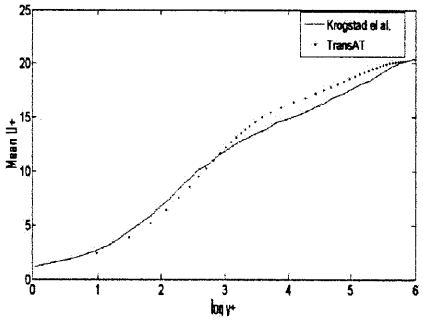

(a)

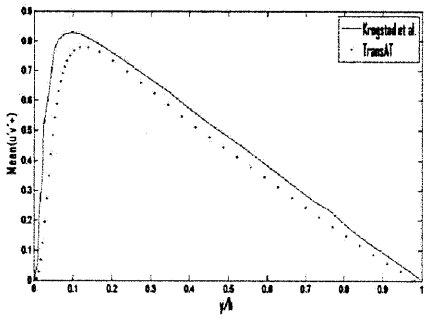

(b)

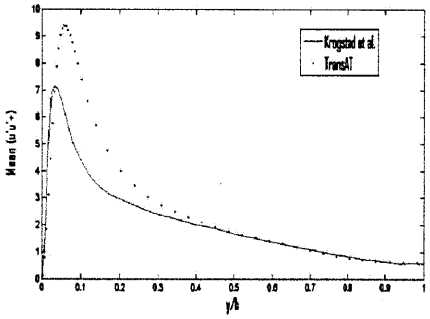

(c)

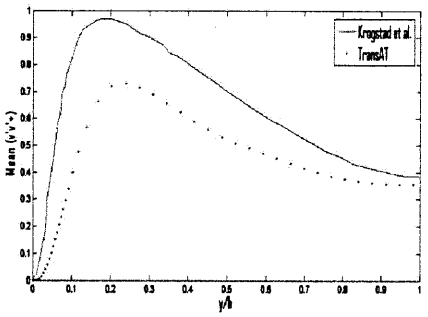

(d)

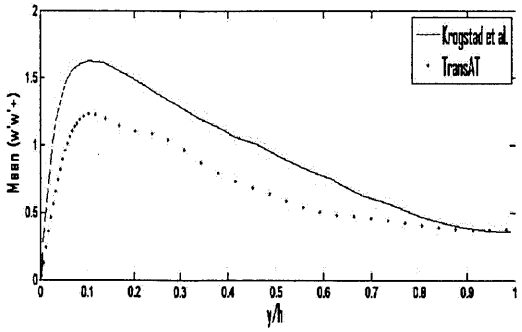

(e)

Figure 6: Normalized velocity profiles and Reynolds stress components obtained with LES in TransAT compared with DNS by Krogstad et al. [51]

6. RESULTS AND DISCUSSION

6.1 Simulation Details:

The geometry used is a horizontal rectangular channel as shown in Figure 7. Perhaps the most serious challenge in modeling wavy stratified and annular flow simulations via LES and DNS methods is the appropriate selection of the boundary conditions. It is not possible to simulate the full BWR fuel channel via DNS and LES methods, as it is computationally very expensive. The Kolmogorov length scale for a standard operating BWR can be shown to be of the order of 1 μm (as shown in appendix A). The number of grid points required to simulate a full BWR channel are of the order of 10^{15} (appendix A) and hence it is not feasible to simulate the full BWR channel as the computational requirements are very high.

It was noted in section 2 that annular and stratified flows are characterized by a large disturbance wave, which is periodic in nature. This fact can be utilized to simulate the developed part of the flow by using periodic boundary conditions. However, in order to get accurate insight into the flow physics, it is necessary to simulate at-least one full wavelength of disturbance wave.

For stratified flow, the wavelength is small and hence it can be easily simulated. As the flow regime transitions to annular flow, the wavelength increases and it was found that simulating even just one full wavelength of annular flow is computationally very challenging but still possible. This will be discussed in individual sections on horizontal stratified and annular flow simulations. In the span-wise direction, periodic boundary conditions are used to eliminate the effects of modeling turbulence near the walls.

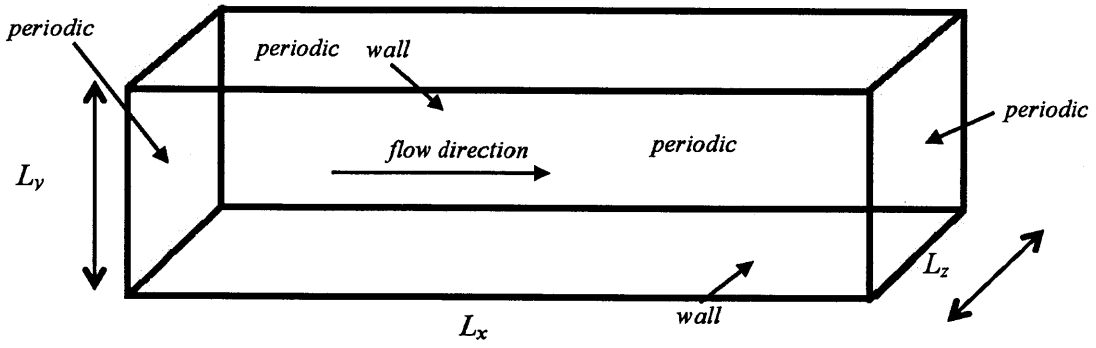

Figure 7: Simulation Geometry with Boundary Conditions

Table 4 shows the simulation parameters used for simulation of stratified and annular flow. In order to initiate the simulation, a slightly perturbed liquid film corresponding to expected void fraction is applied as initial condition. This is shown schematically in Figure 8. The grid used for each of these simulations is structured Cartesian and it is refined near the walls. It is schematically shown in Figure 9. The number of grid points used is different for different simulations and this will be discussed separately for each case. The mean turbulent kinetic energy inside the channel is chosen as one indicator of the convergence of the simulation. The other parameter used to assess the system's convergence is the artificially modeled pressure forcing term.

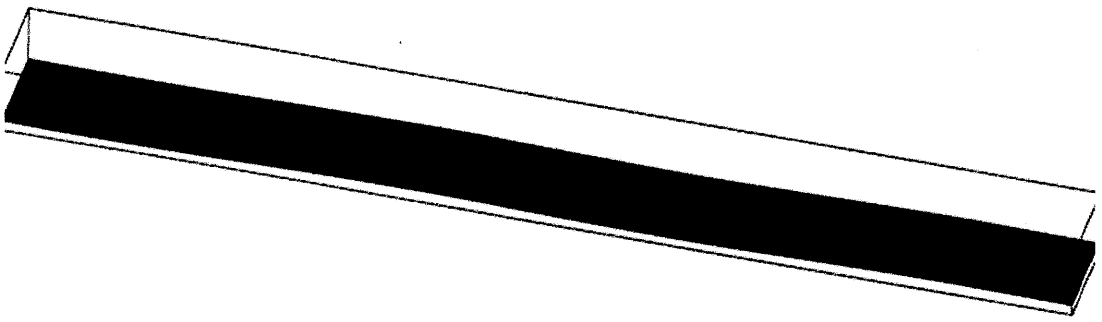

Figure 8: Initial Conditions for LES simulation

Table 4: Simulation Characteristics for Stratified And Annular Flow Simulations

Turbulence + Multiphase Modeling	LEIS
Boundary Conditions	No slip at wall, Periodic in streamwise and spanwise directions
Initial Conditions	Perturbed Film Corresponding to expected Void Fraction for given superficial velocities
Timestep	Adaptive, CFL range between 0.1 and 0.3
Solution Scheme	Explicit for Stratified and Truncated Annular Flow
Pressure Solver	SIP preconditioned GMRES
Grid	Structured Cartesian
Grid Refinement	Local Refinement Near the Wall
Level Set Advection Scheme	WENO 4th order

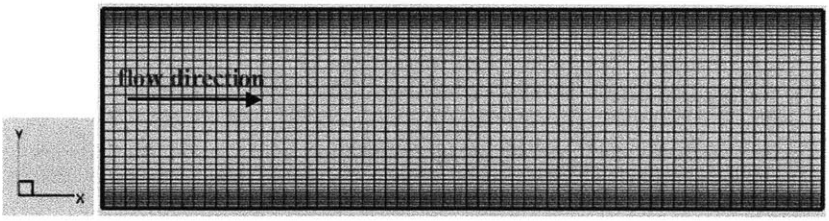

Figure 9: Typical grid used for LES simulations.

6.2 Pressure Forcing Correction:

For a specified channel geometry, the two-phase horizontal channel flow is controlled by the following four parameters:

- Liquid Superficial Velocity, J_l
- Vapor Superficial Velocity, J_g
- Local Void fraction, α
- Pressure gradient, dP/dx

It is noted that specifying both J_g and J_l is equivalent to specifying a combination of mass flux and steam quality for a given mixture. In order to uniquely specify the problem, it is necessary to fix two of the above four parameters. The other two parameters are calculated by the code.

The use of periodic boundary conditions in stream-wise direction imposes an overall pressure drop equal to zero. This leads to a reduction in superficial velocities and the flow tends to stagnate, as there is no force driving the flow. In the "real" situation, the superficial velocities would remain constant while in the "artificial" situation, they are reduced to zero. Hence, our basic strategy is to introduce an effective pressure gradient which maintains keeping the liquid and vapor superficial velocities constant. The liquid and vapor superficial velocities are specified at the beginning of the simulation and an artificial source (external forcing) term is introduced in the Navier-Stokes (N-S) equations and continuously adjusted to keep the superficial velocities constant. As the flow converges to a stable solution, this source term converges too. The convergence of this correction term is used as one of the criteria for convergence of the simulation. The pressure forcing correction is implemented in the following manner:

- Given the superficial velocities for the two phases, the total volumetric flow rate is kept constant by introducing a source term in the N-S equations.

- Additionally the resulting superficial velocity of the liquid is calculated at every time step and the level-set function is adjusted globally (adding or subtracting a small distance, in a time-relaxed manner) such that the desired superficial velocity for the liquid is obtained.

The implementation of the artificial forcing term in TransAT was conducted by Ascomp [53].

The use of such a forcing method also helps in efficient comparison of the simulation to experiments, as typically in experiments the superficial velocities are maintained constant by pumps and/or compressors. It also helps in a simpler and direct comparison of results with the literature as void fraction and pressure gradients are typically correlated with liquid and vapor superficial velocities rather than the other way around.

The code outputs a net pressure forcing term at every time step. This term gives an indication of average acceleration of the system. Denoting this term by a_p, the mixture (photographic) density by ρ and length of the channel in stream-wise direction as L, the average pressure drop ΔP in the channel is given by

$$\Delta P = \rho a_p L \tag{6-1}$$

Using this information, it is also possible to estimate the average interfacial drag. Applying a momentum balance in the stream-wise direction to the control volume (as shown in Figure 10),

$$\frac{d}{dt}(m_{core}u) = \dot{p_{in}} - \dot{p_{out}} + m_{core}a_p - 2F_i \tag{6-2}$$

Here, $\boldsymbol{m_{core}}$ is the mass of vapor core (including droplets), u is the velocity in stream-wise direction, $\boldsymbol{\dot{p}_{in}}$ and $\boldsymbol{\dot{p}_{out}}$ are the rates of momentum inflow and outflow, $\boldsymbol{a_p}$ is the acceleration due to pressure forcing correction term and $\boldsymbol{F_i}$ is the interfacial drag force.

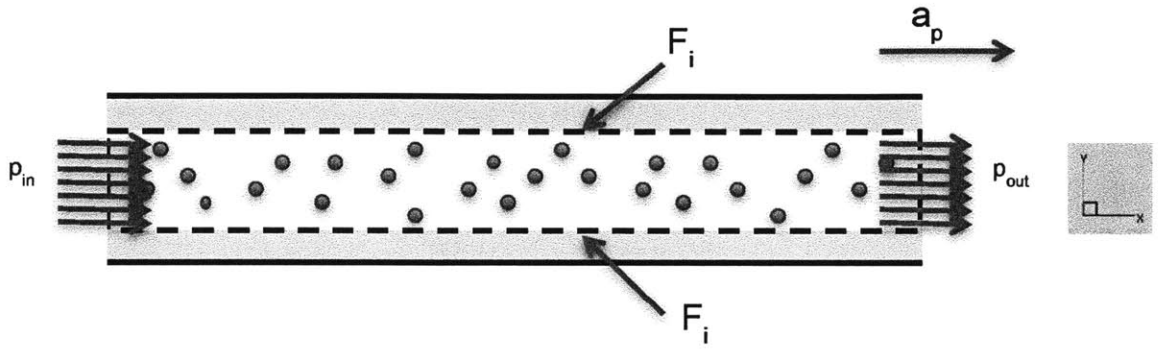

Figure 10: Interfacial Drag for Annular Flow

When the flow is fully-developed, the time-average change of momentum is zero, $d(Mu)$ / dt =0. Also, the use of periodic boundary conditions entails that $\dot{p_{in}} = \dot{p_{out}}$. Hence, equation 6-2 reduces to:

$$F_i = \frac{m_{core} a_p}{2} \tag{6-3}$$

This interfacial force can then be used to calculate the interfacial shear stress and interfacial friction factor as indicated by equations 6-4 and 6-5.

$$\tau_i = \frac{F_i}{A_{film}} \tag{6-4}$$

$$\tau_i = \frac{1}{2} f_i \rho_g j_g^2 \tag{6-5}$$

This formulation for calculation of interfacial drag is slightly different for stratified flow as is evident from Figure 11. The only difference is that the wall shear force needs to be taken into account here as well. Applying the same formulation as that for annular flows,

$$F_i = m_{core} a_p - F_{gw} \tag{6-6}$$

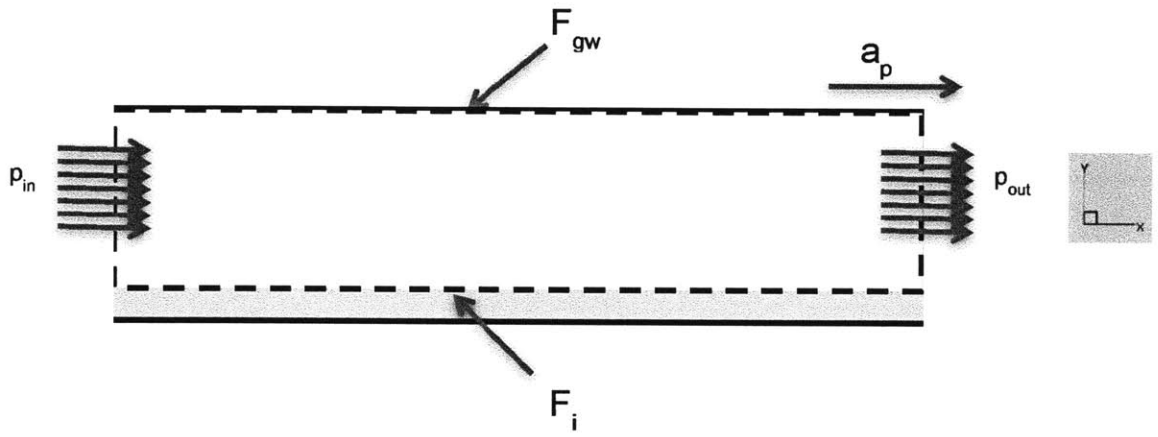

Figure 11: Interfacial Drag for Stratified Flows

Here, F_{gw} is the average gas-wall shear force available from the simulation. Using the interfacial force F_i, the friction factor and interfacial shear stress can be evaluated using equations 6-4 and 6-5.

A study for validation of interfacial shear calculations for stratified flows using the methods suggested above was performed by Ascomp for benchmark case of 2-dimensional two-phase laminar stratified flow flowing through the channel. The geometry and boundary conditions are described in the Figure 12 below. The grid used is 22 x 43 (streamwise x wall normal) and is refined near the walls. There is no pressure gradient and the only driving force is the pressure

forcing term, denoted by a_p. The liquid and vapor Reynolds number, defined by $Re_l = \rho_l j_l H/\mu_l$ and $Re_g = \rho_g j_g H/\mu_g$, are equal to 335 and 313 respectively. The properties of the two phases and geometric parameters are shown in Table 5.

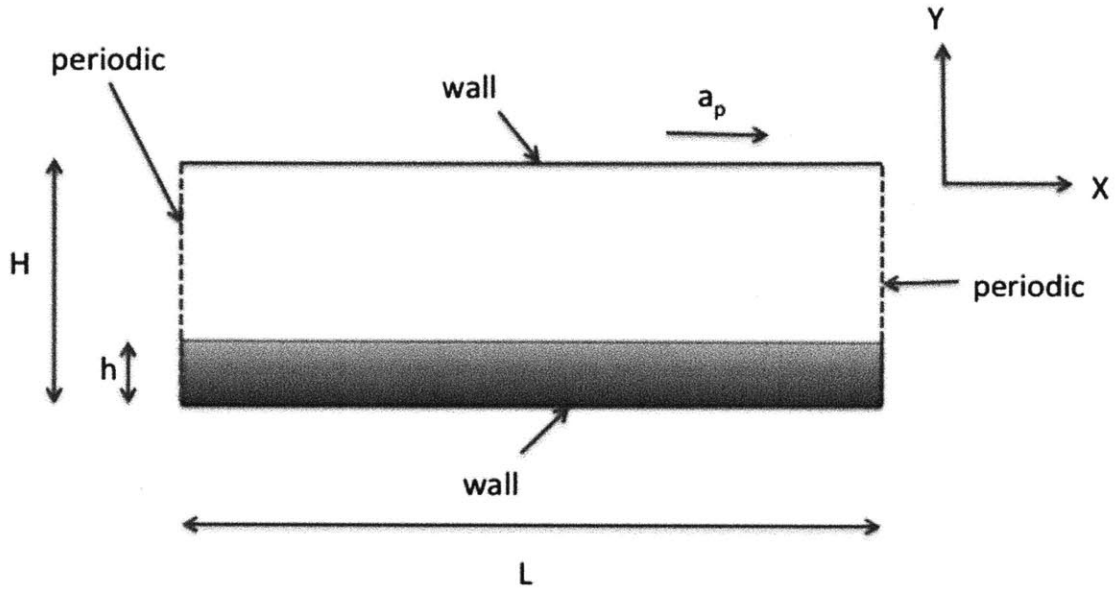

Figure 12: Interfacial Shear Benchmark Case Geometry and Boundary Conditions

Table 5: Properties and Geometric Parameters for Interfacial Shear Benchmark Case

Density of Liquid ρ_l	1000 kg/m^3
Density of Gas ρ_g	1 kg/m^3
Viscosity of Liquid μ_l	0.1 Pa.s
Viscosity of Gas μ_g	0.0018 Pa.s
Surface Tension σ	0.73 N/m
Channel Height H	1 m
Channel Length L	1 m

This case is chosen as a benchmark case as it is possible to obtain an analytical solution for fully developed velocity profile and hence interfacial shear stress for this configuration. The results from this analytical solution are directly compared with results from momentum balance (equation 6-6) to test the accuracy of proposed method.

The four parameters of importance are liquid holdup (*h*), forcing term (a_p), vapor superficial velocity (*jg*) and liquid superficial velocity (*jl*). It is required to fix 2 of these parameters to uniquely specify the problem. The analytical solution is described by equation 6-7 and equation 6-8.

$$u_I = a_p(\rho_l h + \rho_g(H-h))/2\left(\frac{\mu_l}{h} + \frac{\mu_g}{H-h}\right) \tag{6-7}$$

$$\tau_i = \mu_g \frac{u_I}{h-H} - \frac{\rho_g a_p (h-H)}{2} = \mu_l \frac{u_I}{h} - \frac{\rho_g a_p h}{2} \tag{6-8}$$

Here, u_I is the velocity of interface and τ_i is the interfacial shear stress. Table 6 describes the comparison between the analytical solution and momentum balance obtained by fixing a) h and a_p , b) *jg* and *jl*.. It can be seen that good agreement is obtained between interfacial shear calculations from simulation using momentum balance and analytical solution and hence the method for estimation of interfacial shear using momentum balance is accurate.

Table 6: Comparison Between Analytical Solution and Momentum Balance for Interfacial Shear Calculations in Stratified Flow

Parameters Fixed	Value of Fixed Parameters	Value of Parameters Obtained from Simulation	Interfacial Shear from Analytical Solution	Interfacial Shear from Simulation Using Momentum Balance
h and a_p	$h = 0.100$ $a_p = 0.0100$	$j_g = 0.564$ $j_l = 0.0335$	0.003493	0.003533
jg and jl	$j_g = 0.564$ $j_l = 0.0335$	$h = 0.0988$ $a_p = 0.0101$	0.003559	0.003612

* All units are in SI

6.3 Horizontal Stratified Flow Simulations:

As a starting point, stratified flow is modelled for air-water mixture. The results are compared to the measurements of Shi and Kocamustafaogullari [54]. It is noted that Shi and Kocamustafaogullari measured the interfacial parameters in stratified flows in horizontal pipes. However, the simulations are carried out for parallel-plate channel flow geometry (with the same hydraulic diameter) due to their ease of meshing and implementation in TransAT. It is noted that the difference in geometry does not affect the physics of the flow.

Shi and Kocamustafaogullari conducted experiments for a 0.0503 mm inner diameter pipe having a length of 15.4 m and characterized the flow into six regimes based on superficial velocities. Figure 13 represents the flow regime map as described by Shi and Kocamustafaogullari [54] – 2D represents 2-Dimensional, LA represents Large Amplitude and AT represents Atomization. The gas superficial velocity is denoted by Jg and liquid superficial velocity is described by Jf. .To validate the simulations, the wavelength and wave speed measured from the simulations are compared with the results of Shi and Kocamustafaogullari

[54]. Figure 14 shows the wavelength and wave speed as observed by Shi and Kocamustafaogullari for different superficial velocities. In the following subsections, we present the results obtained for 2D regime and Large Amplitude regime identifying the challenges introduced in determining the size of computational domain for each regime. The challenges introduced in modelling the atomization regime are discussed in section 6.3.2. An experimental setup is also developed within the same group to validate these stratified flow results. It is briefly described in appendix B.

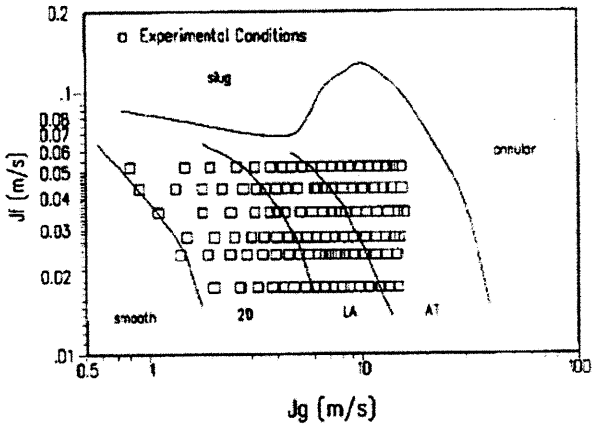

Figure 13: Flow Regime Map (Taken from Shi and Kocamustafaogullari [54])

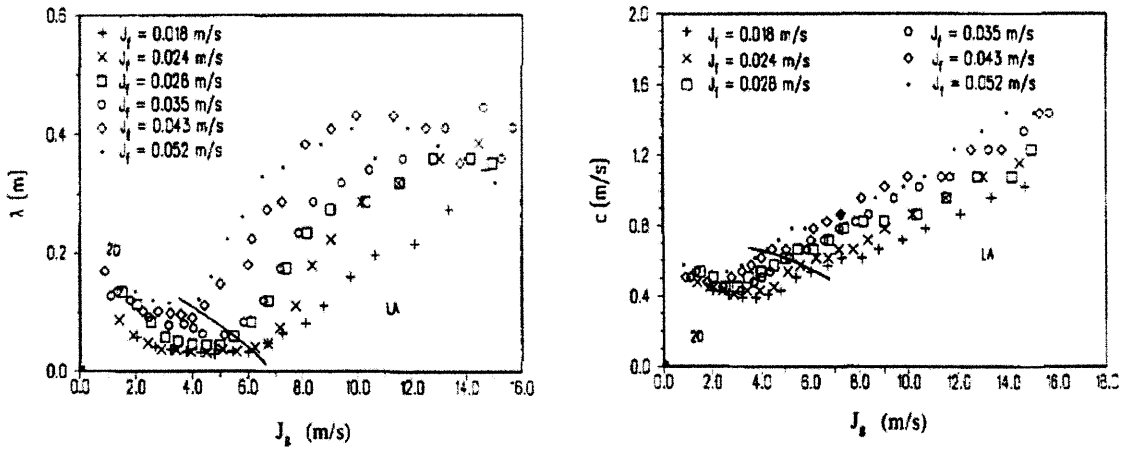

(a) (b)

Figure 14: a) Mean Wavelength, b) Mean Wave Velocity for different gas superficial velocities (taken from Shi and Kocamustafaogullari [54])

6.3.1 2-D Regime:

The vapor superficial velocity is kept at 2 m/s while the liquid superficial velocity is kept at 0.028 m/s. It can be seen from Figure 13 that this falls in the 2D regime. From Figure 14a, it can be seen that the expected wavelength is 0.11 m. This leads to a choice of domain of length 0.12 m in the streamwise direction. The grid used is 100 x 100 x 100 (streamwise x wall normal x spanwise). It is noted that the number of grid points limits the computational resources and hence longer domains (implying larger number of grid points) cannot be used. The choice of domain length is strictly governed by the expected wavelength. A coarse grid is used in the spanwise directions because 2D nature of the flow is expected from experiments. A square cross section of the channel with the side of square equal to 0.0503 m is used.

The wave velocity computed from the simulation in the converged state is 0.6 m/s while it is expected to be 0.5 m/s from Figure 14b and hence shows relatively good agreement. For this

simulation, the in-house experimental setup (appendix B) gives a velocity of 0.4345 m/s. Furthermore, as shown in Figure 15a, the domain consists of only 1 wave spanning its entire length and hence corresponding to a wavelength of 0.12 m which is in relatively good agreement with results reported in Figure 14a.

6.3.2 Large Amplitude Regime:

The vapor superficial velocity in this case is kept at 6.8 m/s while the liquid superficial velocity is fixed to 0.024 m/s. As can be seen from Figure 13, this corresponds to Large Amplitude regime. The expected mean wavelength as seen from Figure 14a is 0.04 m. This leads to a choice of domain of length 0.1 m in the streamwise direction with a grid of 100 x 100 x 125. It is noted that in this case a three dimensional film is expected and hence the grid in spanwise direction is slightly finer than the case described in Subsection 6.3.2. The cross section is the same as the one described for 2D regime. The wave velocity computed from the simulation is 0.8 m/s and expected from Shi and Kocamustafaogullari [54] is 0.6 m/s. It was not possible to use the in-house experimental setup to conduct this run as the in-house setup has a maximum limit of 5 m/s for vapour superficial velocity. At the final converged state (shown in Figure 15b), the mean wavelength observed from the simulation is 0.035m and the expected wavelength from Shi and Kocamustafaogullari [54] is 0.04 m, therefore reasonable agreement is observed between the Shi and Kocamustafaogullari [54] and simulated data.

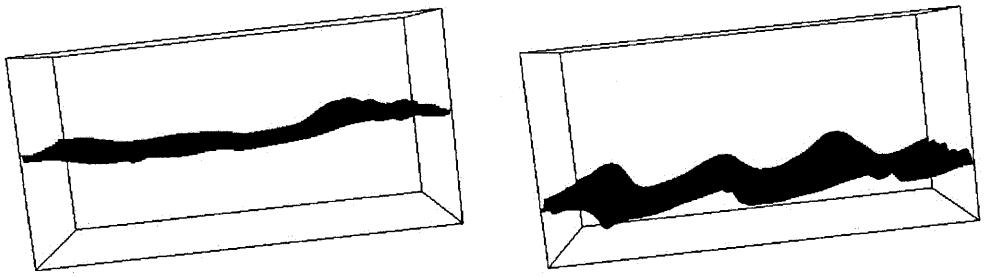

(a) (b)

Figure 15: Wave profile for a) 2-D regime, b) Large Amplitude Regime

6.4 Horizontal Annular Flow Simulations:

From Figure 13 and Figure 14a, it can be inferred from the trends that the wavelengths are significantly larger for the atomization and annular flow regimes than for the 2D and large-amplitude regimes. Therefore, these regimes require a longer domain and hence larger number of grid points and large computation resources. Owing to high computational requirements, the simulations for this regime are carried out in two categories: truncated annular flow simulations and full domain annular flow simulation. The "truncated" domain annular flow simulation refers to the case in which domain length is significantly less than the wavelength of disturbance wave, whereas "full" domain refers to the case in which domain length is similar to the wavelength of disturbance wave.

6.4.1 Truncated Annular Flow Simulations:

As a starting point for modeling annular flows, liquid entrainment for steam-water mixture at 7 MPa in a horizontal channel is modelled. The domain length is 0.01 m in the wall normal direction, 0.02 m in the spanwise direction and 0.025 m in the streamwise direction. The grid is

50 x 100 x 125 (wall normal x spanwise x streamwise). The length of the domain is less than the wavelength of disturbance waves observed from the experiments. The average superficial velocities of both phases are fixed (1.5 and 20 m/s for the liquid and vapor phase, respectively). Figure 16 shows a snapshot of the 3D interface geometry for a preliminary simulation. The gravity is along negative Y direction, X is the streamwise direction and Z is the spanwise direction. In the figure, ligament formation and droplet entrainment are clearly visible. It can be seen that we start with a horizontal stratified flow, which rapidly develops with time into annular flow, and a film is formed on the top surface, which is physically correct. This simulation was carried out on an 8 core 3.00 GHz Intel Xeon CPU X5472 machine with 16 GB RAM. It is however noted that the domain in stream-wise direction is truncated and it does not cover 1 mean wavelength.

(a)

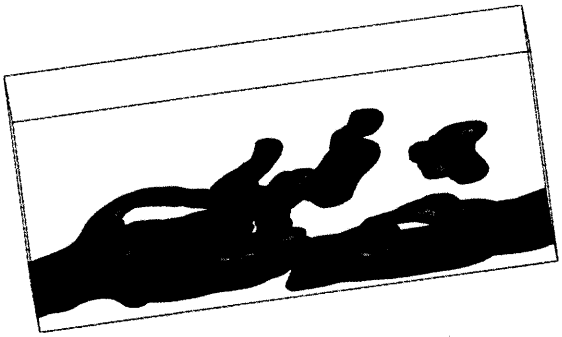

(b)

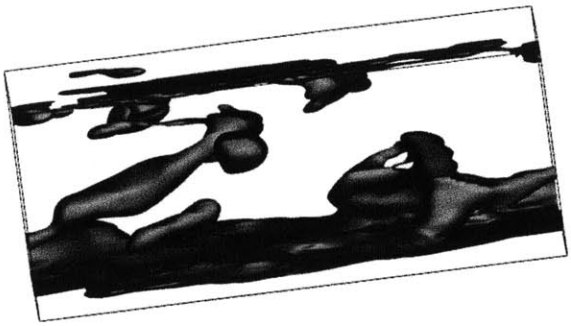

(c)

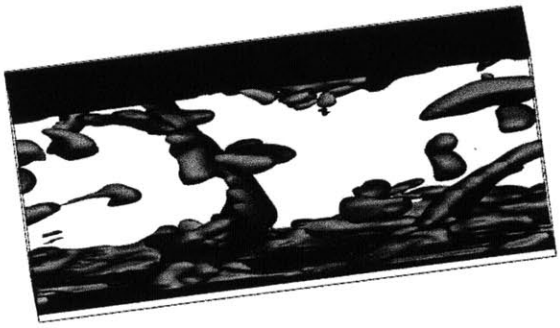

(d)

Figure 16: Truncated Annular Flow Simulation at a) t=0 ms, b) t=20 ms, c) t=40 ms, d) t=80 ms

It is noted here that steam-water mixture at 7 MPa is used in annular flow simulations. The steam-water mixture has a lower liquid to vapor density ratio than air-water mixture. Hence, it improves the performance of level set in capturing interfacial instabilities and characteristics of annular flow.

It was not possible to compare the wavelengths and wave speeds for annular flow regime as a truncated domain is used.

6.4.2 Full Domain Annular Flow Simulation:

This simulation is carried out using multi-block version of TransAT and can be run on high performance computing clusters. The liquid and vapor superficial velocities used were 1.5 m/s and 20 m/s. This simulation corresponds to the test case described in truncated annular flow simulation (section 6.4.1, however, the domain length in stream-wise direction in this case is similar to expected wavelengths of large disturbance waves. Hence, the results from this full domain simulation are used for direct comparison with truncated annular flow simulation. The domain length in the streamwise direction in this case is 0.2 m. The total number of grid points are 10 million (100 x 100 x 1000) distributed over 960 blocks. In terms of implementation, everything else is the same as described in Subsection 6.4.1. At the time of writing this thesis, this simulation is still running.

Figure 17 shows the snapshot of 3D geometry. Figure 18 shows a snapshot of cross-sectional views for this channel coloured with stream-wise velocity magnitude. It can be seen that the ligament formation, interfacial instabilities and droplet formation is clearly captured. At the time of writing this thesis, this simulation is still running and has not fully converged yet. Hence, a film on top surface is not seen. However, Figure 17 c),d),e),f) clearly indicate that liquid droplets are hitting the top surface and a film is being formed.

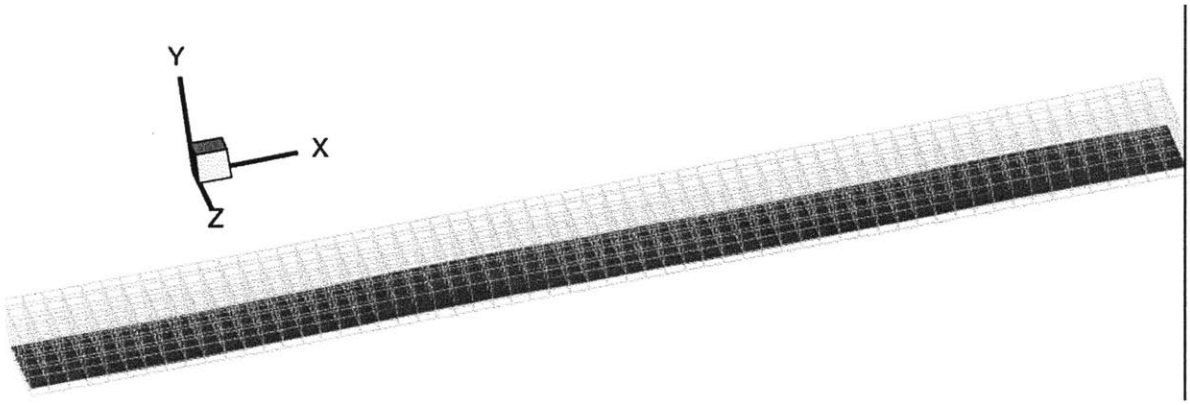

(a)

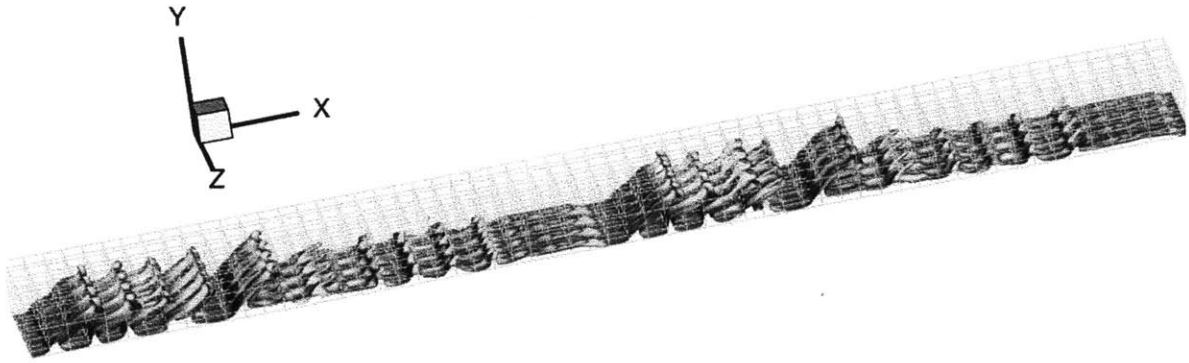

(b)

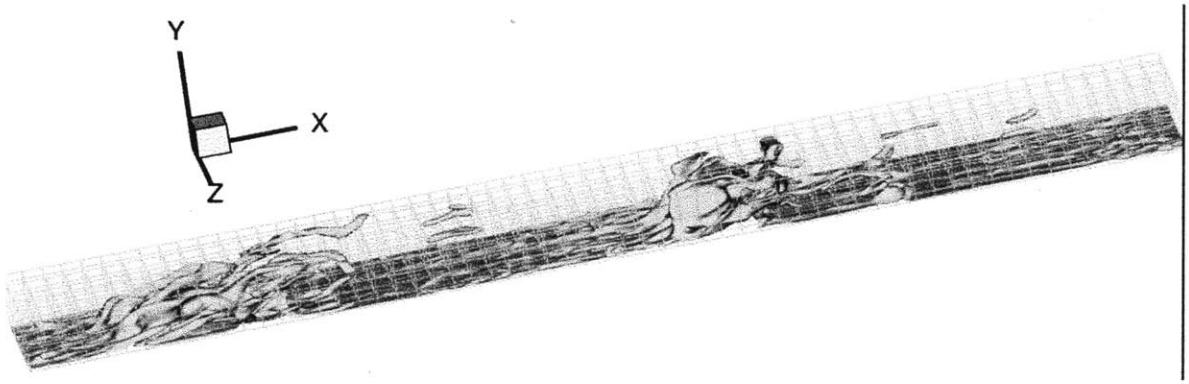

(c)

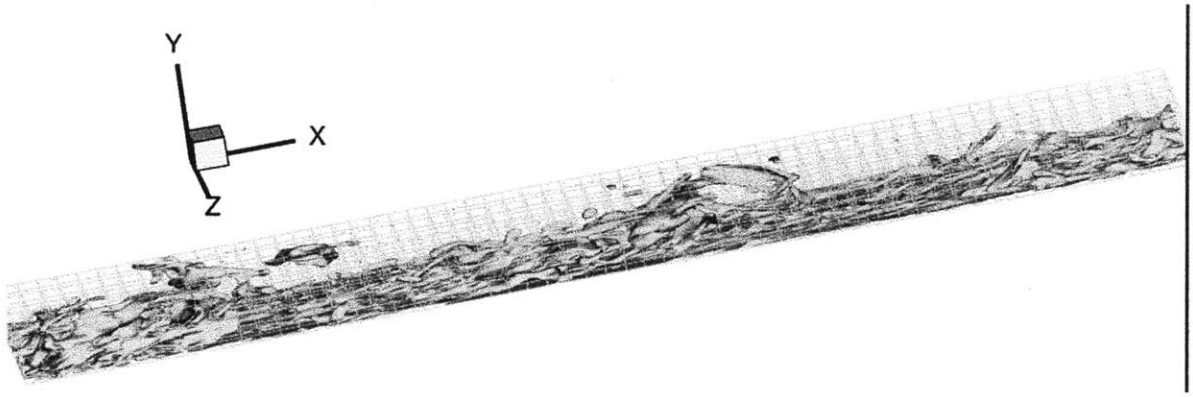

(d)

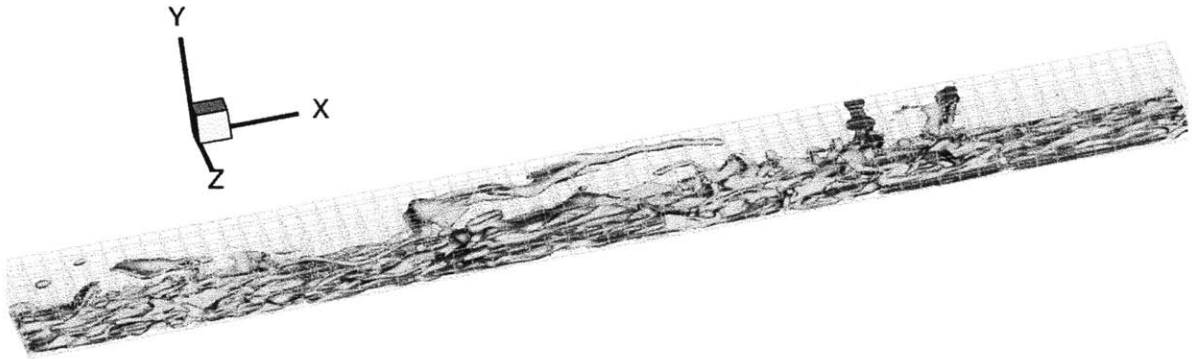

(e)

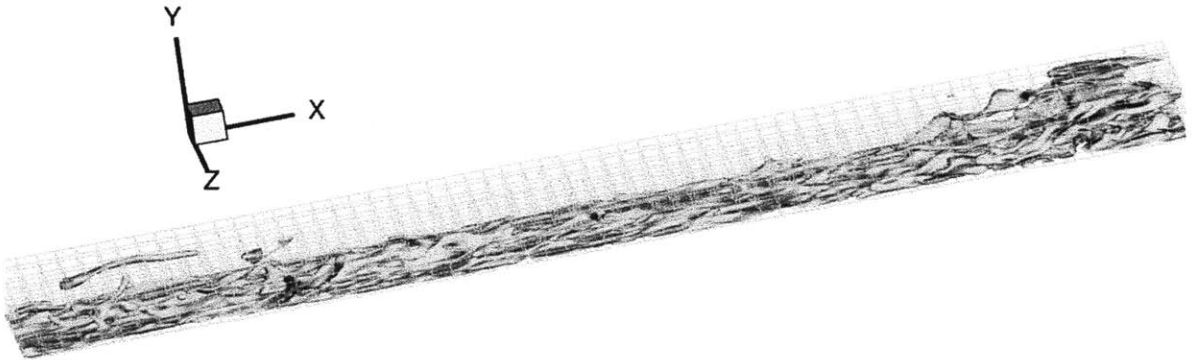

(f)

Figure 17: Full Domain Simulation at a) t = 0 ms, b) t = 5.8 ms, c) t=33.1 ms, d) t=78.9 ms, e) t=108.1 ms, f) t=133.4 ms

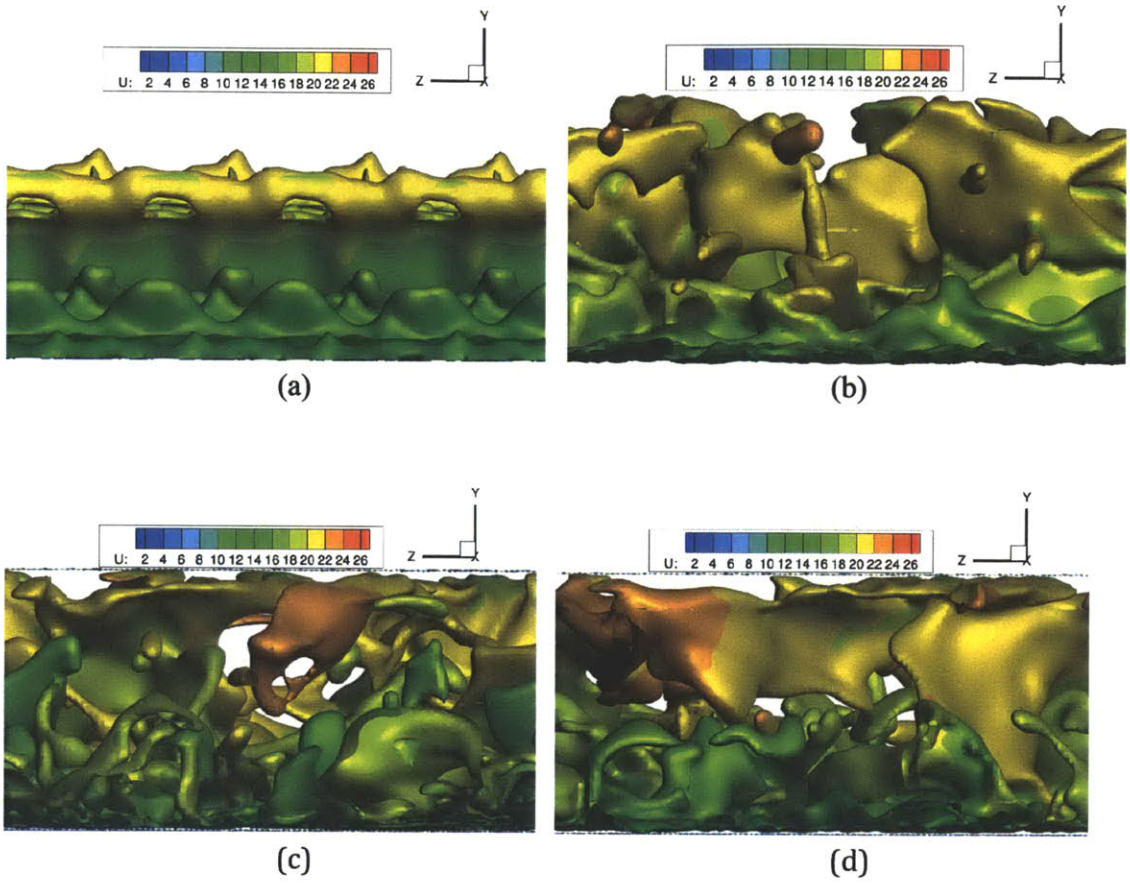

Figure 18: Cross Sectional View of Full Domain Simulation at a) t = 5.8 ms, b) t=33.1 ms, c) t=78.9 ms, d) t=133.4 ms

6.5 Comparison of Macroscopic Parameters:

Table 7 summarizes the various simulations that were conducted for a given value of superficial velocities. For the purpose of validation, the EPRI correlation of Chexal et al. [55] is used as reference and compared with the void fraction obtained from the simulation at converged state. The pressure gradient measured from the simulation is compared with Friedel correlation [56]. The entrainment fraction obtained for annular flow simulations was compared with the

correlation of Okawa et al. [24]. The interfacial shear was compared with the correlation of Wallis [27].

Table 7: Computational Matrix for Stratified and Annular Flow Simulations

Run No.	Jg	jl	Length in Streamwise Direction	Cross-section	Grid	Mixture	Regime
1	2	0.03	0.05	0.05 x 0.05	100 x 100 x100	Air -water at 1 atm	Stratified Wavy
2	7	0.024	0.1	0.05 x 0.05	100 x 100 x 125	Air-water at 1 atm	Stratified Wavy
3*	25	0.45	0.025	0.01 x 0.02	50 x 100 x 125	Steam-water at 7 MPa	Annular
4*	5.5	0.75	0.025	0.01 x 0.02	50 x 100 x 125	Steam-water at 7 MPa	Annular
5*	20	1.5	0.025	0.01 x 0.02	50 x 100 x 125	Steam-water at 7MPa	Annular
6	20	1.5	0.2	0.01 x 0.02	100 x 100 x1000	Steam-water at 7MPa	Annular

*denotes that the domain length in stream-wise direction is less than one wavelength
** All units are SI

It can be seen that the void fraction shows better agreement for steam-water mixture than air-water implying that level set performs better in this case due to a lesser difference in properties. It can be seen that the void fractions are in relatively good agreement with Chexal et al. [55] correlation. The error in void fraction in general from the simulation can be attributed to these four factors: a) loss in mass due to use of periodic boundary conditions in streamwise and spanwise direction, b) loss in mass of liquid due to level set and pressure correction methods, c) loss in mass due to inability of the grid to resolve small interfacial structures and droplets , d) use of a truncated domain length in stream-wise direction, as it does not allow efficient transfer of

mass and momentum by large disturbance wave. The overall results from the simulation give correct qualitative trends and relatively good agreement with the experimental correlation.

The overall trends in pressure gradient calculations obtained from the simulations are similar to those for void fractions, except case 5. Cases 1-4 show relatively good agreement with Friedel correlation[56]. The discrepancy in case 5 can be explained by the fact that a truncated domain in stream-wise direction is used (to keep computational resources tractable) and hence the LES does not perform well as it does not correspond with the topology of the flow. It is seen that case 6 (full domain) performs much better and predicts a larger pressure gradient as the domain is increased.

The entrainment fraction is over-estimated by the simulations for each of the truncated domain simulation. However, it can be seen that the entrainment fraction is of the same order as that is expected by Okawa et al. [24]. The interfacial shear stress calculated from simulation also shows relatively good agreement with Wallis correlation [27] for truncated annular flow simulations. However, a clear discrepancy is seen in simulations for horizontal stratified flow as to the interfacial shear.

It can be clearly seen that the interfacial shear is larger for case 6 than case 5 and much closer to the empirical correlation. Overall, the comparison between case 5 (truncated domain) and case 6 (full domain) clearly indicates that as the domain length gets closer to that of the observed disturbance wave, the quality of results obtained from simulations of annular flow becomes much better.

Table 8: Comparison of Macroscopic Parameters Obtained from Stratified and Annular Flow Simulations

Run. No.	Void Fraction from Chexal et al [55]	Void Fraction LEIS	Pressure Gradient from Friedel correlation[56]	Pressure Gradient LEIS	Entrainment Fraction from Okawa et al[24]	Entrainment Fraction LEIS	Interfacial Shear from Wallis [27]	Interfacial Shear LEIS
1	0.66	0.821	38.05	188.37	-	-	0.6564	0.07933
2	0.81	0.902	90.61	213.71	-	-	4.4688	0.09676
3*	0.996	0.963	19548.5	13168.10	0.96	0.876	61.83	65.52
4*	0.78	0.852	3803.74	3839.93	0.73	0.801	8.97	16.97
5*	0.858	0.916	21731	3461.02	0.94	0.853	46.88	17.09
6	0.858	0.893	21731	8909.5	0.94	0.888	46.88	44.23

*denotes that the domain length in stream-wise direction is significantly less than one wavelength
* All units are SI

Properties for air-water at 1 atm

	P	Density	Viscosity
Air	1 bar	1.2 kg/m^3	0.0000178 Pa·s
Water	1 bar	1000 kg/m^3	0.001137 Pa·s
Surface Tension		0.073 N/m	

Properties for steam-water at 7 Mpa

	P	Density	Viscosity
Steam	7 MPa	36.52 kg/m^3	0.00001896 Pa·s
Water	7 MPa	736.72 kg/m^3	0.00009124 Pa·s
Surface Tension		0.01763 N/m	

7. CONCLUSION AND FUTURE WORK

A Computational Multiphase Fluid Dynamics based simulation framework of liquid entrainment in BWRs is developed using a combination of LES for turbulence and ITM for interface evolution. ITMs avoid the usage of empirical correlations and assist in modeling of annular flows using first principles. This can help gain insightful information about the physics of problem and also obtain more accurate models without making oversimplifying assumptions and conservative approximations.

The CMFD simulations in this work are performed with the code TransAT. In this study, the interface tracking and turbulence modeling capabilities of TransAT were tested using representative benchmark cases of two-dimensional wavy falling liquid films with large interfacial deformation and turbulent single phase channel flows. The results from the simulations on two-dimensional wavy falling liquid films were in good agreement with results obtained by Nosoko et al. [50] and Nave [5]. The results of Krogstad et al. [51] were used for validation of simulations on turbulent single-phase channels. The code predicts results in reasonable agreement with the data reported in the literature.

The main challenge identified in modeling BWR fuel channels is the boundary conditions. It was shown that it is impossible to model the full BWR channel via LES and DNS methods using existing computational resources, as it requires nearly 10^{15} grid points. However, it was shown that it is possible to simulate fully developed conditions by intelligent application of periodic boundary conditions in stream-wise direction to a

portion of fully–developed flow domain containing at least one large disturbance wave. Stratified and annular flows are characterized by a mean disturbance wavelength responsible for transfer of momentum and in order to fully capture the physics, the domain should at least be as long as this wavelength.

The use of periodic boundary conditions implied automatic development of new algorithms to take the distortion in geometry into account. Periodic boundary conditions automatically render pressure gradient across the channel to be zero and hence an appropriate pressure forcing term was developed to simulate the real condition.

Before moving on to modeling of annular flows, horizontal wavy stratified flows were modeled. For the purpose of validation of horizontal wavy stratified flows, the experimental data set of Shi and Kocamustafaogullari [54] is used. Limited experimental data from an in-house experimental setup is also used for validation. Comparisons are made for data points lying in 2D wavy and Large Amplitude Regimes, and it is seen that the wave speed and wavelength are fairly well predicted by the simulations. The study of horizontal stratified flows again emphasizes the need of choosing domain for CFD simulations.

Annular flows have larger wavelengths than stratified flows and hence have a larger domain. It turns out that simulation of even one full wavelength requires extensive computational resources. Hence, annular flow simulations were split up into two categories – truncated annular flow (domain less than one wavelength and full domain

annular flow simulation (domain similar to full wavelength). A comparison of macroscopic parameters such as void fraction, pressure drop, interfacial drag and entrainment fraction were performed for each simulation. A comparison of truncated and full domain annular flow simulation was also performed and it was found that the full domain annular flow simulations give a much better agreement with empirical correlations than truncated domain simulations.

In this study, the entrainment and deposition rates are not calculated. Accurate calculation of entrainment rates would involve tracking of droplets, and it would mean switching to a Lagrangian approach. Also, the framework for full domain simulation can be used for getting more and more data and providing a comparison with existing correlations. This work does not include heat transfer, however, evaporation is also an important component of dryout. As an addition to the existing framework, heat transfer can be implemented in the CMFD model as well.

Accurate models for dryout conditions in BWRs can significantly help in reduction of safety margins and hence an increase in operating power densities. Annular flows and stratified flows also find significant use in pipeline operations in oil industry. It is very clear that CMFD modeling of such kind of flows has a very strong economic incentive and it could greatly help in reduction of cost of energy.

8. REFERENCES

[1] Todreas, N.E. and Kazimi, M., (2011), Nuclear Systems Volume I: Thermal Hydraulic Fundamentals, Second Edition, *Taylor & Francis.*

[2] Secondi, F., (2009), An Assessment of Entrainment Correlations for the Dryout Prediction in BWR Fuel Bundles, *13th International Topical Meeting on Nuclear Reactor Thermal Hydraulics (NURETH-13).*

[3] Hoyer, N., (1998), Calculation of dryout and post-dryout heat transfer for tube geometry, *International Journal of Multiphase Flow, Volume 24, Issue 2, Pages 319-334.*

[4] Prosperetti, A. and Tryggvason, G., (2007), Computational Methods for Multiphase Flow, *Cambridge University Press.*

[5] Nave, J.C., (2004), Direct Numerical Simulation of Liquid Films, *PhD Thesis, University of California Berkeley.*

[6] Woodmansee, D.E. and Hanratty, T.J., (1969), Mechanism for the removal of droplets from a liquid surface by a parallel air flow, *Chemical Engineering Science, Vol. 24 (2), pp. 299-307.*

[7] Whalley, P.B., (1987), Boiling, condensation, and gas liquid flow, *Oxford University Press.*

[8] Tatterson, D.F., Dallman, J.C., Hanratty, T. J., (1977), Drop Sizes in Annular Gas-Liquid Flows, *AICHE Journal 23(1), pp. 68-76.*

[9] Barbosa Jr., J.R., Hewitt, G.F., Konig, G., Richardson, S.M., (2002), Liquid Entrainment, Droplet Concentration and Pressure Gradient at the onset of annular flow in a vertical pipe, *International Journal of Multiphase Flow, 28, 943-961.*

[10] Ishii, M. and Mishima, K., (1984), Two Fluid Model and Hydrodynamic Constitutive Relation, *Nuclear Engineering and Design, 82 (2-3), pp. 107-126.*

[11] Ishii, M. and Mishima, K., (1989), Droplet Entrainment Correlation in Annular Two-Phase Flow, *International Journal of Heat and Mass Transfer, vol. 32, No. 10, pp. 1835-1846.*

[12] Barnea, D. (1987) A unified model for predicting flow-pattern transitions for the whole range of pipe inclinations, *Int. J. Multiphase Flow*, 13, 1-12.

[13] Taitel and Dukler, A.E., (1976), A model for predicting flow regime transitions in horizontal and near horizontal gas-liquid flow, *AIChE Journal, vol. 22, pp. 47-55.*

[14] Azzopardi, B.J., (1998), Drops in Annular two phase flow, *International Journal of Multiphase Flow, 23, 1-53.*

[15] Azzopardi, B.J., Wren, E., (2004), What is entrainment in vertical two phase churn flow? , *International Journal of Multiphase Flow, 30, 89-103.*

[16] Hewitt, G.F. and Hall-Taylor, N.S., (1970), Annular Two-Phase Flow, *Oxford, New York, Pergamon Press.*

[17] Kataoka, I. and Ishii, M., (1983), Entrainment and Deposition Rates for Droplets in Annular Two Phase Flow, *ASME-JSME Thermal Engineering Joint Conference, Honolulu, Hawaii*

[18] Sawant, P., Ishii, M., Mori, M., (2009), Prediction of amount of entrained droplets in vertical annular two phase flow, *International Journal of Heat and Fluid Flow 30, 715-728.*

[19] Sawant, P., Ishii, M., Mori, M., (2008a), Droplet entrainment correlation in vertical upward co-current annular two phase flow, *Nucl. Eng. Des. 238(6), 1342-1352.*

[20] Lopez de Bertodano, M.A., Assad, A., Beus, S., (1998), Entrainment rate of droplets in the ripple annular regime for small vertical ducts, *Nuclear Science and Engineering, Vol. 129 (1), pp. 72-80.*

[21] Pan, L., Hanratty, Thomas J., (2002), Correlation of entrainment for annular flow in vertical pipes, *International Journal of Multiphase Flow, 28, 363-384.*

[22] Dallman, J.C., Jones, B.G., Hanratty, Thomas J., (1979), Interpretation of entrainment measurements in annular gas-liquid flows, *AIChE Symp. Ser 2, 68-76.*

[23] Kataoka, I., Ishii, M., Nakayama, A., (2000), Entrainment and deposition rates of droplets in annular two phase flow, *International Journal of Heat and Mass Transfer, 43, 1573-1589.*

[24] Okawa, T., Kotani, A., Kataoka, I., Naitoh, M., (2004), Prediction of the critical heat flux in annular regime in various vertical channels, *Nuclear Engineering Design, 229, pp. 223-236.*

[25] Hewitt, G.F. and Govan, A.H., (1990), Phenomenological Modeling of Non-Equilibrium Flows with Phase Change, *International Journal of Heat Mass Transfer, vol. 33, 2, pp. 229-242.*

[26] Utsuno, H. and Kaminaga, F., (1998), Prediction of liquid film dryout in two-phase annular mist flow in an uniformly heated narrow tube, *Journal of Nuclear Science Technology, 35, 9, pp. 643-653.*

[27] Wallis, G.B., (1969), One Dimensional Two-Phase Flow, *McGraw-Hill, New York.*

[28] Patruno, L.E., Marchetti, J.M., Jakobsen, H.A., Svendsen, H.F., (2009), Modeling of Droplet Entrainment in Annular Two Fluid Three Phase Dispersed Flow, *13th International Topical Meting on Nuclear Reactor Thermal Hydraulics (NURETH-13).*

[29] Corre, J.M.L. and Adamsson, C., (2009), Development of a New Mechanistic Tool for the Prediction of Liquid Film Dryout During a Transient, *13th International Topical Meting on Nuclear Reactor Thermal Hydraulics (NURETH-13).*

[30] Hizoum, B., Saha, P., Andersen, J.G.M. and Whitlow, K., (2011), Droplet Entrainment and Deposition Rate Models for Determination of Boiling Transition in BWR Fuel Assemblies, *14th International Topical Meting on Nuclear Reactor Thermal Hydraulics (NURETH-14).*

[31] Michta, E., Fu, K., Anglart, H., Angele, K., (2011), Numerical Predictions of Bubbly Two-Phase Flows with OpenFOAM, *14th International Topical Meting on Nuclear Reactor Thermal Hydraulics (NURETH-14).*

[32] Yao, W. and Morel, C., (2004), Volumetric Interfacial Area Prediction in Upward Bubbly Two-Phase Flow, *International Journal of Heat and Mass Transfer, Vol. 47, pp. 307-328.*

[33] Damsohn, M. and Prasser, H.-M., (2011), Experimental Droplet Deposition Distribution Downstream of Functional Spacers in an Adiabatic BWR Mockup

Model, *14th International Topical Meting on Nuclear Reactor Thermal Hydraulics (NURETH-14).*

[34] Lahey, R., (2005), The Simulation of Multidimensional Multiphase Flows, *Nuclear Engineering and Design, 235, 10-12, pp. 1043-1060.*

[35] Rodriguez, J.M., (2009), Numerical Solution of Two Phase Annular Flow, *PhD Thesis, Rensselaer Polytechnic Institute.*

[36] Lakehal, D., Meier, M., Fulgosi, M., (2002), Interface tracking towards the direct simulation of heat and mass transfer in multiphase flows, *International Journal of Heat and Fluid Flow, 23, pp. 242-257.*

[37] Tryggvason, G., Zaleski, S., Scardovelli, R., (2011), Direct Numerical Simulations of Gas-Liquid Multiphase Flows, *Cambridge University Press.*

[38] Drew, D.A. and Passman, S.L., (1999), Theory of Multicomponent Fluids, *Springer, New York.*

[39] Anderson, D.M., McFadden, G.B., Wheeler, A.A., (1998), Diffuse Interface Methods in Fluid Mechanics, *Annual Review of Fluid Mechanics, 30, pp. 139.*

[40] Chella, R. and Vinals, J., (1996), Mixing of a Two Phase Fluid by Cavity Flow, *Physics Review E., 53/4, pp. 3832.*

[41] Brackbill, J.U., Kothe, D.B., Zemach, C., (1992), A Continuum Method for Modelling Surface Tension, *Journal of Computational Physics, 100, pp. 335.*

[42] Meier, M., Yadigaroglu, G., Smith, B.L., (2002), A Novel Technique for Including Surface Tension in PLIC-VOF Methods, *Eur. J. Mech. B: Fluids, 21, pp. 61.*

[43] Rider, W.J. and Kothe, D.B., (1998), Reconstructing Volume Tracking, *Journal of Computational Physics, 141, pp. 112.*

[44] Fedkiw, R. P., Aslam, T., Merriman, B., Osher, S., (1999), A non-oscillatory Eulerian Approach to Interfaces in Multi-material Flows (The Ghost Fluid Method), *Journal of Computational Physics, 152 (2), pp. 457.*

[45] Sussman, M. and Smereka, P., (1997), Axisymmetric Free Boundary Problems, *Journal of Fluid Mechanics, 341, pp. 269.*

[46] Pope, S.B., (2000), Turbulent Flows, *Cambridge University Press.*

[47] Lakehal, D., (2008), LEIS for the Prediction of Turbulent Multifluid Flows with and without Phase Change Applied to Thermal Hydraulic Applications, *XCHD4NRS OCDE Conf., Grenoble.*

[48] Liovic, P. and Lakehal, D., (2007b), Multi-Physics Treatment in Vicinity of Arbitrarily Deformable Fluid-Fluid Interfaces, *J. Comp. Phys., 222, pp. 504-535.*

[49] Reboux, S., Sagaut, P., Lakehal, D., 2006, Large Eddy Simulation of Sheared Interfacial Two-Fluid Flow, *Phys. Fluids 18 (10), 105105.*

[50] Nosoko, T., Yoshimura, P.N., Nagata, T., Oyakawa, K., (1996), Characteristics of Two Dimensional Waves on a Falling Liquid Film, *Chemical Engineering Science, Vol. 51, Issue 5, pp. 725-732.*

[51] Krogstad, P.A., Andersson, H.I., Bakken, O.M., Ashrafian, A., (2005), An experimental and numerical study of channel flow with rough walls, *Journal of Fluid Mechanics, Vol. 530, pp. 327-352.*

[52] Kravchenko, A.G., Moin, P., Moser, R., (1996), Zonal Embedded Grids for Numerical Simulations of Wall-Bounded Turbulent Flows, *Journal of Computational Physics, 127, pp. 412-423.*

[53] Narayanan, C. and Caviezel, D., (2011), Private Communication.

[54] Shi, J. and Kocamustafaogullari, G., (1994), Interfacial Measurements in Stratified Flow Patterns, *Nuclear Engineering and Design 149, pp. 81.*

[55] Chexal, B., Lellouche, G., Horowitz, J., Healzer J., (1992), A Void Fraction Correlation for Generalized Applications, *Progress in Nuclear Energy, Vol. 27, No. 4, pp. 255-295.*

[56] Friedel, L., (1979), Improved friction pressure drop correlations for horizontal and vertical two-phase pipe flow, *European Two-Phase Flow Group Meeting, Ispra, Italy, paper E2.*

APPENDIX A

ESTIMATION OF KOLMOGOROV LENGTH SCALES IN BWR

The standard BWR geometric parameters and operating conditions adapted from Todreas and Kazimi [1] are shown in the following table:

Table 9: BWR Operating Conditions

Pressure (P)	7 MPa
Core Flow Rate ($\dot{M}$)	13.1 Mg/s
Channel Length (L)	4.1 m
Inlet Temperature (T_{in})	278
Average Linear Heat Rate ($\dot{q}$)	19.0 kW/m
Fuel Pin Pitch (p)	0.0162 m
Pin Diameter (d) – This includes clad	0.0131 m
No. of fuel pins per assembly (N_p)	62
No. of Assemblies (N_A)	748
No. of Water Rods per assembly (N_W)	2
Outer Diameter of Water Rod (d_w)	0.0249 m
Channel Box Inner Dimension (a_l)	0.139 m

Using the information in Table 9 and properties for saturated steam at 7 MPa, the BWR operating parameters described in Table 10 can be calculated.

Table 10: Typical BWR Parameters Calculated from Operating Conditions

Parameter	Relevant Equation	Value
Average Mass flow rate through each channel ($\dot{m}_A$)	$\dot{m}_A = (1 - 0.1)\frac{\dot{M}}{N_A}$ *Assuming an average bypass fraction of 10%	15.76 kg/s
Flow Area Through the Assembly (A_A)	$A_A = a_l^2 - \frac{N_p \pi d^2}{4} - \frac{N_w \pi d_w^2}{4}$	0.009995 m^2
Average Mass flux through each sub-channel (G)	$G = \frac{\dot{m}_A}{A_A}$	1576.79 kg/(m^2s)
Area of sub-channel (A)	$A = \left(p^2 - \frac{\pi d^2}{4}\right)$	0.000128 m^2
Wetted Perimeter (P_w)	$P_w = \pi d$	0.0411 m
Hydraulic Diameter (D)	$D = \frac{4A}{P_w}$	0.0125 m
Inlet Enthalpy (h_{in})	Steam Tables	1225.30 kJ/kg
Exit Enthalpy (h_{out})	$h_{out} = h_{in} + 2\dot{q}L/(\dot{\pi}GA)$ *Assuming a cosine shaped power profile	1471.14 kJ/kg
Exit Flow Quality (X)	$X = \frac{h_{out} - h_f}{h_g - h_f}$	0.163
Exit Vapor Superficial Velocity (j_g)	$j_g = \frac{GX}{\rho_g}$	7.06 m/s
Exit Liquid Superficial Velocity (j_l)	$j_l = \frac{G(1-X)}{\rho_l}$	1.79 m/s

The integral length scale of the problem is hydraulic diameter, and the integral velocity scale for phenomenon occurring inside liquid film is liquid superficial velocity. The integral length scales denote the scale of largest eddy within the liquid film. Hence, average dissipation rate (and average production rate) of turbulence can be estimated as:

$$\epsilon \sim \frac{j_l^3}{D} \tag{A-1}$$

Hence, the Kolmogorov Scales can now be calculated as shown below:

$$\eta = \left(\frac{\nu_l^3}{\epsilon}\right)^{\frac{1}{4}} = 0.831\times10^{-6}m \tag{A-2}$$

Hence, in order to fully resolve the flow via DNS methods, the approximate number of grid points needed to resolve the full BWR channel can be estimated using the following equation:

$$N_{gridpoints} = \frac{AL}{\eta^3} = 9\times10^{14} \tag{A-3}$$

APPENDIX B

EXPERIMENTAL SETUP FOR HORIZONTAL STRATIFIED FLOW

The schematic of experimental setup is shown in **Figure 19**. The test section is a rectangular tube with an aspect ratio of 1:3 (15 mm x 45 mm) and is made of borosilicate. The hydraulic diameter is 22.5 mm, which is similar to that of BWR (16 mm). Since the length of rectangular channel is about 4 m, channel supports are needed to provide additional stability to the channel. An injection channel with a form of a frustum of quadrangular pyramid is installed to ensure a relatively larger injection hole. This injection channel is made of plastic by using Stereolithography technique. A flow divider is also attached to injection flange to separate both fluids and ensure fully developed flow. Water flows from water tank and circulates in closed loop. However, the air runs through flow divider and channel with once-through system.

High speed camera records stratified flow inside flow channel for 3 seconds with 1,000 frames per second. Some LED lights are located under flow channel to supply enough light when using high speed camera. Flow meters for air and water are installed to measure respective flow-rates. The flow meters can measure air superficial velocity from 0.7 m/s to 5.0 m/s and a maximum water superficial velocity of 0.065 m/s. **Figure 20** shows a sample image obtained from high speed camera for jg=2 m/s and jl=0.028m/s. The images obtained for fully developed region from high speed cameras are analyzed using Fourier methods to calculate wave speed, wavelength and wave frequency.

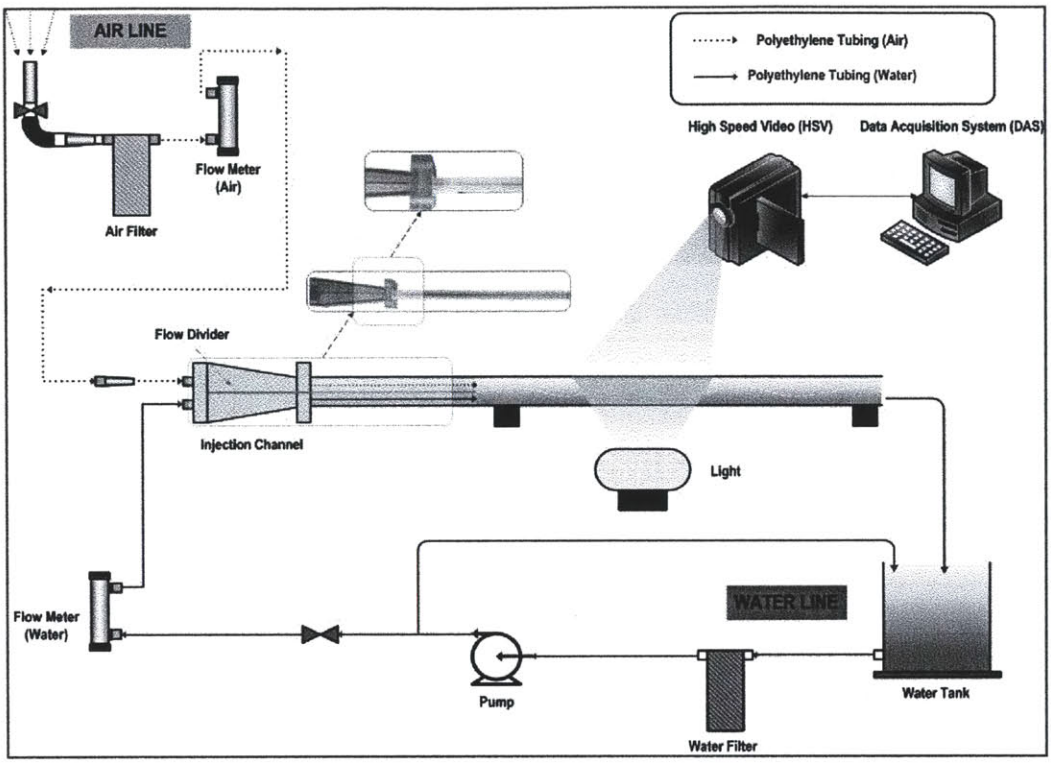

Figure 19: Experimental Setup for Horizontal Stratified Flow

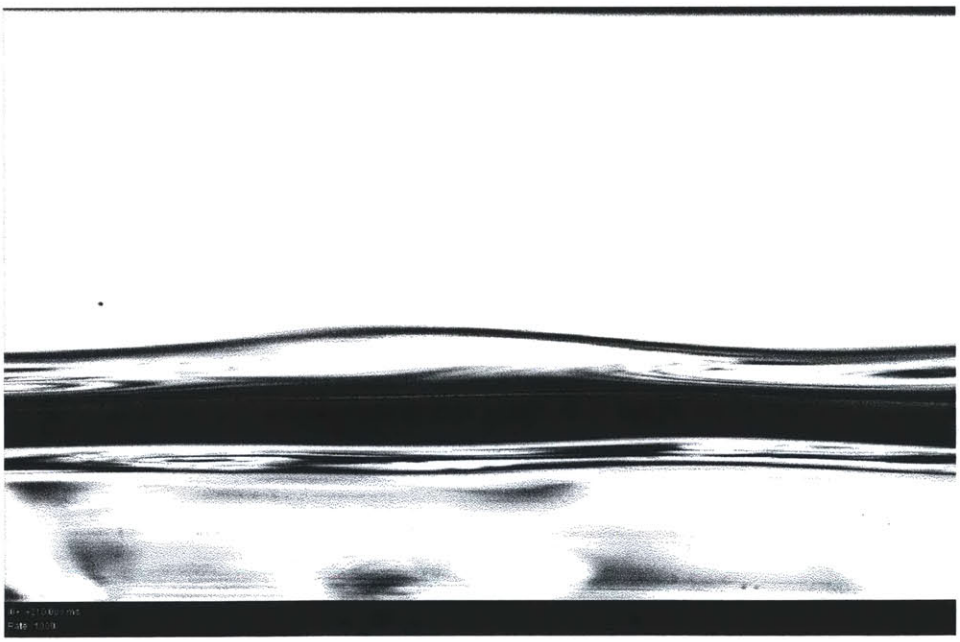

Figure 20: Sample Image from High Speed Camera for Stratified Flow Experiment